UCLouvain

École polytechnique de Louvain

Modelling coral larvae exchanges between the Great Barrier Reef and outer reefs

Author: **Noé Desmet**
Supervisors: **Emmanuel Hanert, Éric Deleersijder**
Readers: **Jonathan Lambrechts, Olivier Carlier d'Odeigne**
Academic year 2018–2019
Master [120] in Civil Engineering

Acknowledgements

I would like to address my first thanks to my supervisor Emmanuel Hanert. His positivism and his interest in my work have always remained a great source of motivation. Even in more complicated moments, when I was dealing with incoherent errors in the code, when that prevented me from producing any advancement for days, sometimes weeks he was always encouraging and present. Meeting twice a week on its own is exceptional and was extremely helpful to me.

I enjoyed working on this subject, and I thank my co-supervisor Eric Deleersnijder for giving me solid basis in marine hydrodynamics.

I also thank Thomas Dobbelaere and Antoine Saint-Amand for sharing their experience and their time (but also their scripts). They particularly saved me precious time in setting up the model code. I include in this acknowledgement all the members of the SLIM team who advised and helped me.

Thanks to my fellow workers Jessica, Nicolas and François for their support. A special thanks to Robin that helped me every time I faced a new obstacle, up until the last days before submission. Finally I thank my sister who read over my English even if this thesis is far from her area of expertise and my family for their unwavering support throughout my studies.

Contents

1 Introduction

1.1 Coral reefs: what to know

First thing to know about coral is that even if the coral reefs cover less than 0.1% of the area of the ocean, they produce an ecosystem so rich that they support more than 25% of all marine species living on this planet. In fact, coral reefs provide shelter for a variety of life that rivals the one associated with the Amazon rainforest.

The impacts of sheltering this abundance of life are many and varied. It is established that dozens of millions of people rely on them for nutrition and livelihoods. Global estimates suggest that they provide some 375 billions of dollars worth of goods and services around the globe each year [Costanza et al. , 1997]. A major ecosystem service provided by the reefs is coastal protection. They reduce the effects of a storm on the coastlines by absorbing wave energy by an average of 97% [Ferrario et al. , 2014], avoiding flood damages worldwide and saving lots of expenses in artificial defences (e.g. breakwaters) or in damage repairs.

All these reasons justify that we protect and preserve these life-sustaining natural wonders, especially knowing that their own equilibrium is so fragile. Indeed they are currently facing an ecological crisis all around the world.
Corals depend upon a symbiotic relationship with unicellular micro-algae called zooxanthellae. These micro-algae, living within the tissues of the corals, are the ones responsible for their coloration. The corals provide them with CO_2 and ammonium allowing the algae to photosynthesize. In return they get the nutrients they need to live, grow and expand in reef-buildings. This relationship turns out to be a crucial factor for the tropical corals living in clear and nutrient-poor water, supplementing 90% of the corals' nutrition [Stanley , 2006].

It turns out that corals and zooxanthellae are very sensitive to water temperature and water acidity. Sea temperatures in many tropical regions have increased these last years so much that the thermal tolerance of corals and their micro-algae has been frequently exceeded during the last decades.
This is when coral bleaching occurs [Hoegh-Guldberg , 1999]. The coral expels the zooxanthellae and therefore loses its principal source of nutrients along with its color. This process makes the white skeleton of the coral visible, hence the term "coral bleaching". When a coral bleaches it is not fatal, it has the ability to survive short-term disturbance but it becomes much more vulnerable to the slightest stress. However, if the conditions that lead to the expulsion of the micro-algae persist, the death of the coral becomes more certain. Long and more frequent periods of bleaching are observed on all tropical coral reefs, leading an increasing part of them to die due to insufficient nutrient intake.

Figure 1.1: Picture of a fire coral that experienced severe bleaching in the 2016 mass bleaching event (GBR). Source figure: Richard Vevers, *The Ocean Agency*

Bleaching is a regional event, it concerns most of the corals living in a region where the conditions cause the micro-algae to be repelled. Although recent years have seen several mass bleaching events in 1998, 2002, 2006, 2016, most recently 2017 and counting according to the AIMS (the Australian Institute of Marine Science). Additionally climate model projections tend to show that these events will be more and more frequent in the future [Hughes et al. , 2018], which is really worrying for the future corals' sustainability.

Climate change, which is induced by rapid buildup of greenhouse gases in the atmosphere, gets sea surface temperatures to rise but also leads to an acidification of the ocean [Carpenter et al. , 2008]. That makes it the bigger driver to bleaching events.
There are in fact a bunch of other triggers, among which is overfishing, that increases zooplankton levels, which in turn causes corals to starve of oxygen. Let's also mention runoff and pollution: major runoff carries pollutants diluting rapidly in ocean water and lead near-shore corals to bleach.

1.2 Subtropical and temperate reefs in Australia

The Great Barrier Reef is the largest and surely the most famous reef ecosystem. It stretches on all the Queensland coast, northeast Australia (see figure 1.2), and covers a plateau of 344 400 km^2 of shallow waters.

Figure 1.2: Map of The Great Barrier Reef Region. Source figure: *World Heritage Area and Marine Park*, 2014

Even if coral reefs are associated with tropical latitudes, there are also a number of locations beyond the tropics where corals proliferate. Among others, these high-latitude sites include West Australia's coasts, Japan or Florida (see figure 1.4) and especially our case: the east Australian coast and its southern reefs.

South to the GBR, for instance on the shores of the Solitary Islands (30°S) or near Lord Howe Islands (31°S), we can find subtropical corals whose growth rates have been studied by V. Harriott [Harriott , 1999]. One can find reefs as far from the tropical latitudes as Sydney. These are deep reefs, historically kelp-dominated even if recent observations that will be discussed below have shown the emergence and growth of tropical coral reefs [Booth and Sear , 2018 & Hannam , 2018]. Those reefs located at the south to the GBR are precisely what we will consider in this study.

The key current that links these different areas is known as the East Australian Current (EAC). Rather famous for its size, high velocities (the flow can reach 90 cm/s) and transport (until 35 Sv[1]) and its impact on the environment, the EAC is the largest ocean current near Australia.

[1] 1 Sv = 1 billion liters per second

It is formed from the South Equatorial Current (SEC) reaching Australia's eastern coast. The SEC is then divided at 15°S, the EAC being the flow proceeding southward. At around 32°S the EAC is in turn split. One part of the flow keeps the direction southward while another forms a northward countercurrent, giving the EAC its U shape [Hamon , 1965].

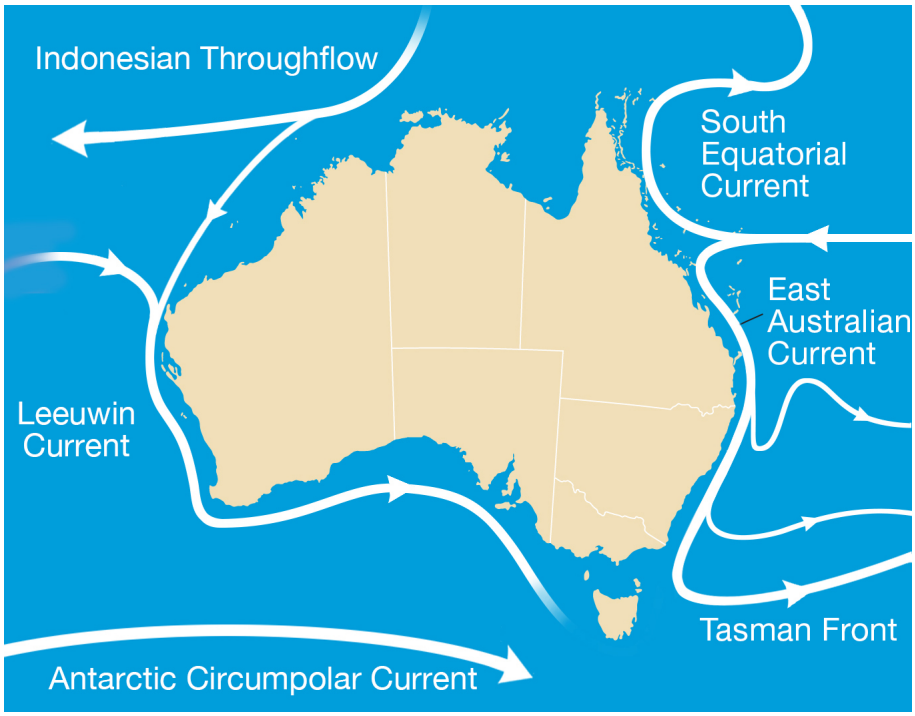

Figure 1.3: Schematic image representing major currents around Australia including the EAC. Source figure: *Bureau of Meteorology (Australian Government)*, 2018

1.3 The importance of subtropical reefs

The subtropical reefs (see figure 1.4) also form biogeographic transition zones. These zones are the first to highlight range shifts and local extinctions due to climate change [Sommer, Harrison, Beger, and Pandolfi , 2014]. It is explained by the fact that many species living in these zones are at the margins of their range and environmental tolerances.

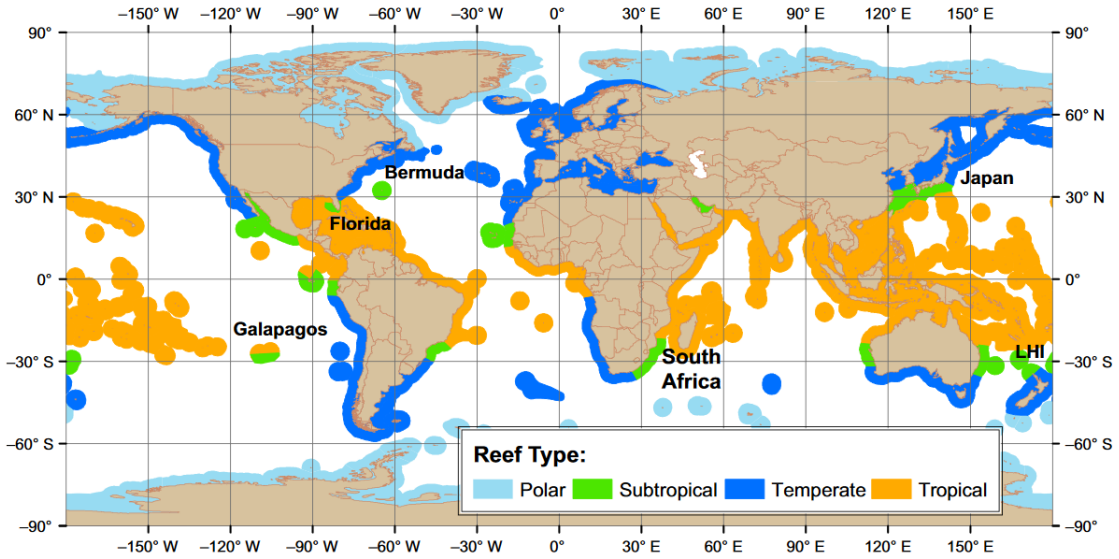

Figure 1.4: Locations of marine bioregions that include subtropical non-accreting reefs supporting scleractinian corals or where tropical and temperate reef biota overlap. Source figure : [Beger et al. , 2014]

If we take our case of subtropical reefs on Australia's eastern coast, we may observe in the same habitat tropical hard corals and fish species from GBR but also temperate kelp and fish species.
This reason alone is enough to pay attention to these zones and preserve them. They are huge natural laboratories, giving a glimpse of the reaction of species from different natural habitat to climate change.

1.3.1 Tropicalisation

At the moment, several shifts of tropical corals and fish species are being noticed. They expand their range poleward, meaning that some tropical fishes overwinter on higher latitudes and that some reefs that were historically kelp-dominated evolve to coral-dominated [Beger et al. , 2014]. The exact conditions leading to this process called "tropicalisation" are diverse but above all, they are not well understood. The presence of tropical coral reefs next to Sydney [Hannam , 2018] is a perfect example of this lack of understanding.

Figure 1.5: The Pocillopora aliciae species of coral is now proliferating off the coast near Manly. Source figure: John Sear, *The Sydney Morning Herald*, 2018

1.3.2 Conservation through time

Hoping that biogeographic transition zones such as subtropical reefs will act as climate change refuges makes this specific type of environment first in line for protection and preservation. Studies like the one lead by Maria Beger [Beger et al. , 2014] evaluate management strategies to preserve both the natural situation of these high-latitude coral reefs and their potential to act as refuges.

1.4 Objective

Climate change and the bleaching that is induced threaten coral reefs ecosystems. Their potential as refuges for tropical species put subtropical reefs at the top of the scientists' concerns.

This paper intends to answer the questions: "can we collect useful information on those subtropical reefs, their connectivity", "is a shift of tropical coral reefs from the GBR to outer, southern reefs possible considering the area's currents ?".

We aim to model coral larvae exchanges in the southern part and between these regions to evaluate their connectivity. To get these answers, we have to achieve three steps:

- Devising a high-resolution ocean model for the Australia's eastern coast (including a part of the GBR)
- Modelling the larval dispersal using a Lagrangian particle tracker

- Extracting information about the connectivity between reefs and interpreting this information using relevant indices

2 Currents simulation

2.1 Existing models

We need to devise an ocean model wide enough to be able to study the coral larvae exchanges in our study area. There are several models in existence such as HYCOM, SLIM or the one provided by eReefs.

HYCOM[2], which stands for HYbrid Coordinate Ocean Model, is a three-dimensional global model developed by the National Ocean Partnership Program (NOPP) as part of the U.S. Global Ocean Data Assimilation Experiment (GODAE). HYCOM is one of the most mature model based on the hybrid coordinates approach [Chassignet et al. , 2007]. The whole idea of hybrid coordinates is to combine isopycnal coordinates in the open, stratified ocean and z-level coordinates in the mixed layer, in shallow coastal regions or/and in unstratified seas [Bleck , 2002]. The results of the model applied on different regions and at different resolutions are available online on the model's website. An interesting application is the Global Ocean Forecasting System (GOFS) with a resolution of 1/12° (more or less 10 km). The resolution is not fine enough to reach our objective.

SLIM[3] is an unstructured-mesh hydrodynamic model that can fully simulate flows, from rivers to coastal oceans. This model is developed at UCLouvain and relies on the discontinuous Galerkin finite element method. It offers many interesting possibilities, allowing to work with 1D, 2D or 3D meshes, to simulate the transport of larvae/debris or the dynamics of tracers by means of a Lagrangian particle tracker and a Eulerian transport model. The use of unstructured mesh has been proved to be pretty robust and capable of handling various types of shallow water flows [Yoon and Kang , 2004].

[2] https://www.hycom.org/

[3] Second-generation Louvain-la-Neuve Ice-ocean Model, https://www.slim-ocean.be/

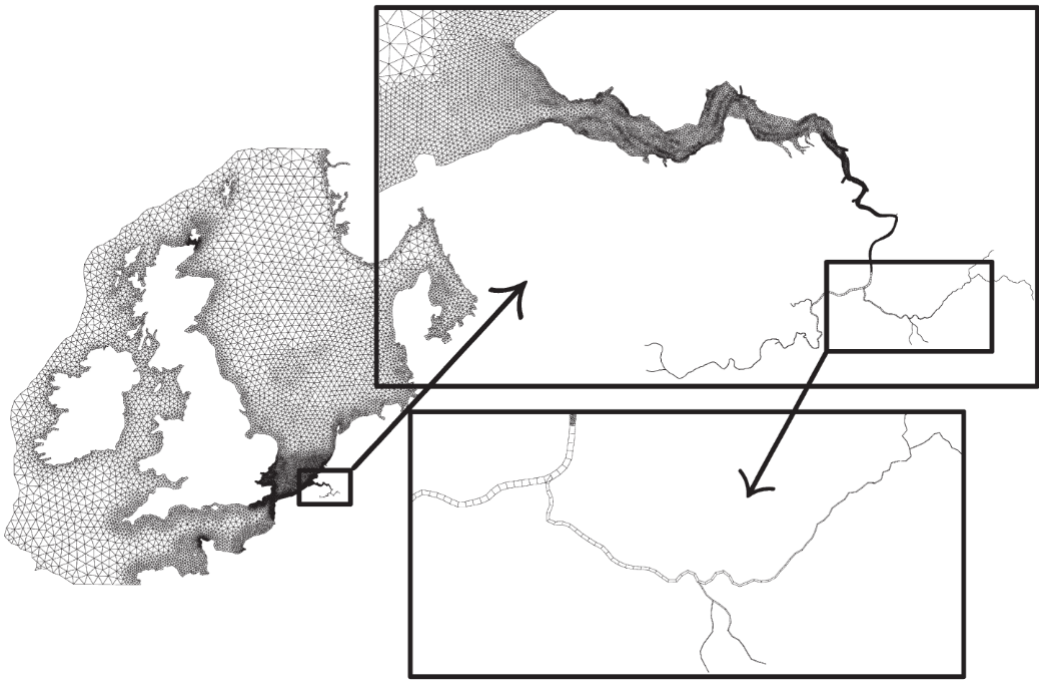

Figure 2.6: Illustration of the unstructured meshes that SLIM allows to use (the river Scheldt, estuary and its tributaries [De Brye et al. , 2010])

It allows to increase the resolution on complex geometry regions (near coasts, reefs,...) while keeping it coarser on deeper and/or on more uniform regions. More specifically, SLIM turned out to be efficient to solve the shallow water equations and to model the flows of varied regions such as estuaries or coastal oceans [De Brye et al. , 2010; Van et al. , 2016; Lambrechts et al. , 2008].

The marine modelling component of eReefs[4] has developed numerical models capable of simulating the hydrodynamics and predicting sediment transport, water quality and basal ecology of the Great Barrier Reef lagoon and reef matrix. Like HYCOM, eReefs data is delivered online. However, the model is applied on the Great Barrier Reef and doesn't cover all our region of interest.

In this study we will then use the 2D barotropic version of SLIM, modelling horizontal velocities. This method has already been used several times in other studies such as [Dobbelaere , 2018; Hanert, Thomas, Lambrechts, Deleersnijder, and Wolanski , 2012]. What we lose in precision by flattening the ocean will be compensated by a high minimal resolution near reefs and coasts.

2.2 Hydrodynamic modelling

The following equations are the non-linear shallow equations of the hydrodynamic model.

[4]https://research.csiro.au/ereefs/

$$\frac{\partial \eta}{\partial t} + \nabla \cdot (H\mathbf{u}) = 0 \tag{2.1}$$

$$\frac{\partial \mathbf{u}}{\partial t} + \mathbf{u} \cdot \nabla \mathbf{u} = -f\mathbf{e}_z \times \mathbf{u} - g\nabla\eta - \frac{g\|\mathbf{u}\|\mathbf{u}}{C^2 H} - C_S \frac{|\mathbf{u} \cdot \nabla H|}{H} \cdot \mathbf{u} + \frac{\tau}{\rho H} + \frac{1}{H}\nabla \cdot [H\nu(\nabla \mathbf{u})] \tag{2.2}$$

where $H = h + \eta$ is the water column depth, h is a reference depth level and η is the variation from this reference depth level, $\mathbf{u}$ is the horizontal depth-integrated velocity, f is the Coriolis factor, $\mathbf{e}_z$ is a unit vector pointing vertically upwards, τ is the surface wind stress, g is the gravitational acceleration, ρ is the water density, ν is the horizontal viscosity, C is the Chezy bottom-stress coefficient and C_S is the numerical slope stress coefficient.

In this study we chose to work with a $\Delta t = 900s$. The results of SLIM are exported every hour.

The bathymetry used is provided by Geoscience Australia and the National Oceans Office. In 2005 they produced a consistent, high-quality 9 arc-second (0.0025° or 250m at the equator) bathymetric grid for Australian waters [Whiteway , 2009]. In 2009 they improved it by including recently acquired datasets but conserving the same "bounding box" between 92°E and 172°E, and 8°S and 60°S. Actually, the 0.0025 dd resolution is only supported where direct bathymetric observations are sufficiently dense [Webster and Petkovic , 2005]. In areas where no sounding data is available, the grid is based on the 2 arc-minute ETOPO [W. H. Smith and Sandwell , 1997] and 1 arc-minute ETOPO [Amante and Eakins , n.d.] satellite derived bathymetry.

To make sure the entire domain is under water at all time, we set the minimum depth to $h = 5m$. Indeed, the shallow water equations can only be solved with positive value of H. An overview of this bathymetry is shown in figure 2.7.

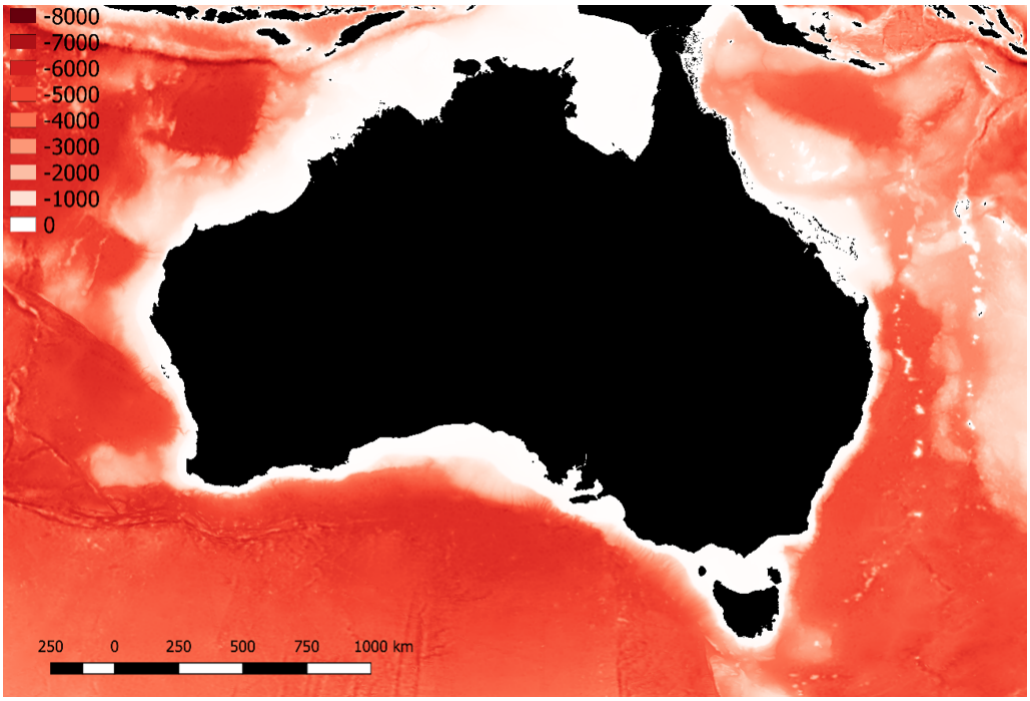

Figure 2.7: The bathymetry around Australia used in our model.

The Chezy bottom-stress coefficient C is defined as : $C = \frac{H^{1/6}}{n}$ where n is the Manning coefficient. We take $n = 0.25m^{-1/3}s$ on reefs and $n = 0.025m^{-1/3}s$ elsewhere, which is the same value as the one used in [De Brye et al. , 2010]. The positions of the reefs are obtained combining two shapefile layers provided by the Great Barrier Reef Marine Park Authority[5] (GBRMPA) and by Maria Beger[6]. The former covers the GBR area with high precision while the latter covers all the eastern coast of Australia (see figure 2.8 and 2.9). Therefore we prefer to use the GBRMPA's file where it is available (on the GBR) and use the one provided by Maria Beger elsewhere. She constructed this last file with all the information she could gather. Even if this results in a heterogeneous file (excellent accuracy in some regions but coarse on others), it is a much valued file (particularly at this stage) and all the credit goes her.

[5]http://www.gbrmpa.gov.au/geoportal/
[6]University Academic Fellow in Marine Conservation Science, University of Leeds

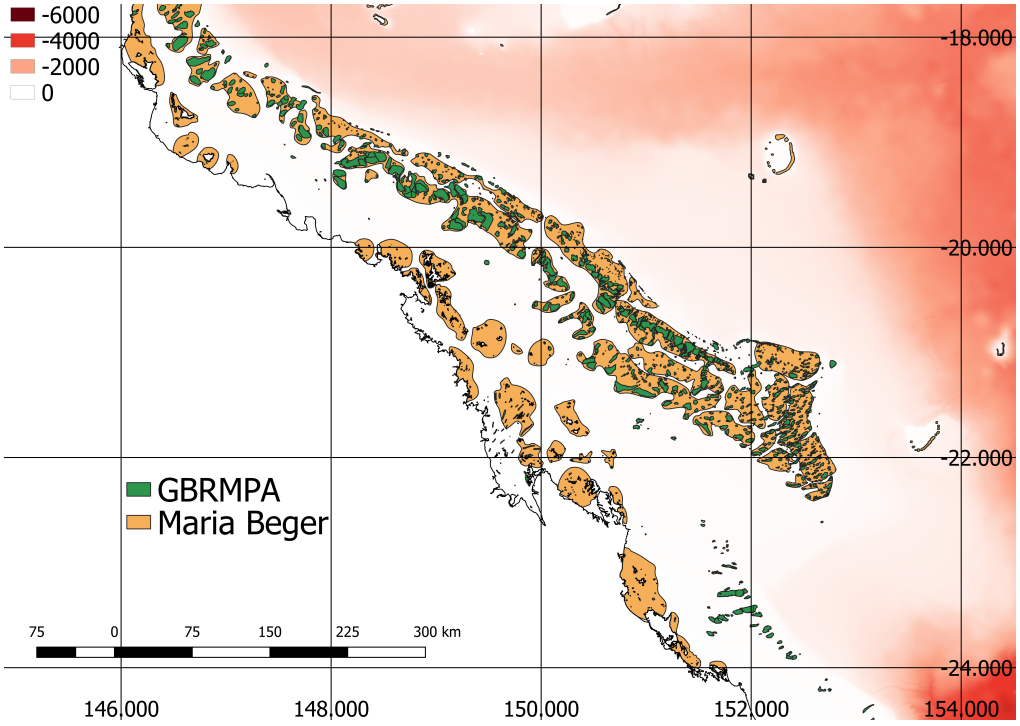

Figure 2.8: The GBRMPA file is used on the GBR because of its much higher resolution.

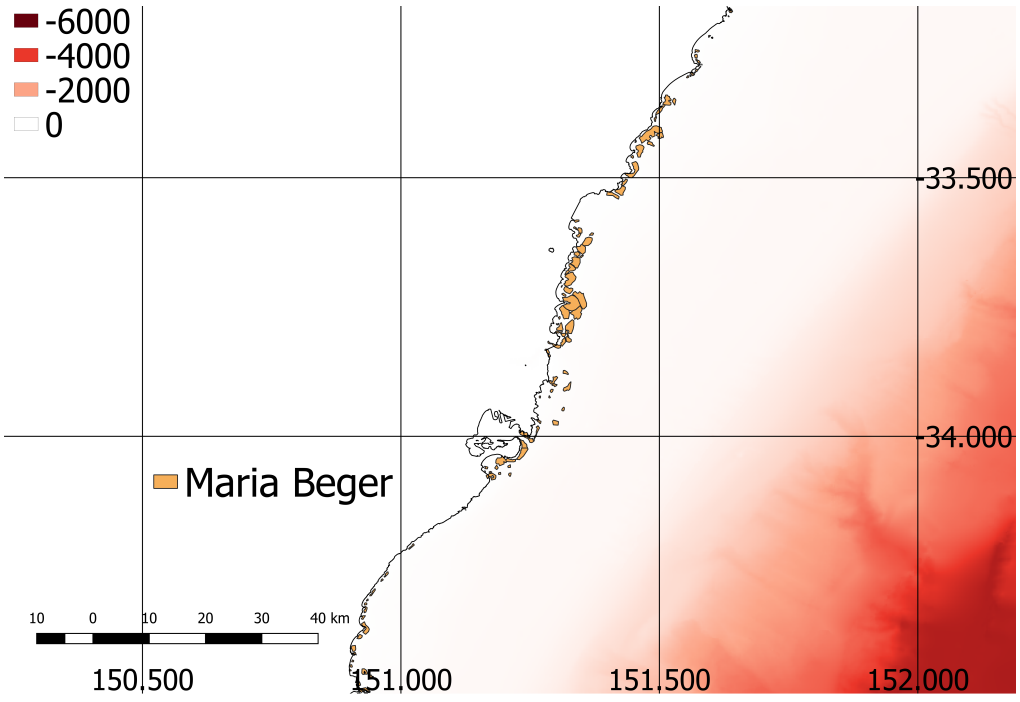

Figure 2.9: The subtropical reefs mapped by Maria Beger are located on the coast in small groups.

This friction term is combined with a slope-dependant friction term. The numerical slope stress coefficient C_S is chosen to be equal to 5 as in the study [Frys , 2018].

The surface wind-stress is computed as follows:

$$\tau = \rho_{air} C_D \|\mathbf{u}_{10}\| \mathbf{u}_{10} \tag{2.3}$$

where ρ_{air} is the air density, C_D is the drag coefficient and $\mathbf{u}_{10}$ is the wind speed (in ms^{-1}) at 10 meters above the sea surface [Cushman-Roisin and Beckers , 2011]. The wind speed data that we will use come from the model CFSv2 (Climate Forecast System) of the National Centers for Environmental Prediction[7] (NCEP). The parametrisation of the drag coefficient C_D takes into account the fact that stronger winds cause rougher sea surface and therefore increase the influence of the wind (the [S. Smith and Banke , 1975] parametrisation).

$$C_D = 10^{-3}(\alpha + \beta \|\mathbf{u}_{10}\|) \tag{2.4}$$

where $\alpha = 0.63$ and $\beta = 6.6 \cdot 10^{-2} m^{-1} s$. This paramatrisation holds valid for wind speeds between 3 and 21 ms^{-1} [Geernaert , 1987]. Our region of interest features winds of this type.

Finally, to take the unresolved turbulent features into account, we applied the Smagorinsky parametrisation [Smagorinsky , 1963] to determine ν:

$$\nu = (\tilde{C}_S \Delta)^2 \sqrt{2\left(\frac{\partial u}{\partial x}\right)^2 + 2\left(\frac{\partial v}{\partial y}\right)^2 + \left(\frac{\partial u}{\partial y} + \frac{\partial v}{\partial x}\right)^2} \tag{2.5}$$

where Δ is the local mesh element size, (x, y) are the Cartesian coordinates of the horizontal plan, (u, v) are the components of the depth integrated velocity $\mathbf{u}$ and the Smagorinsky coefficient $\tilde{C}_S = 0.1$ [Lambrechts et al. , 2008].

2.3 Unstructured mesh

As said above, using an unstructured mesh allows us to use a computational domain larger than the region of interest to keep boundaries away from it. We also adapt the resolution of the mesh: fine on reefs and near the coasts and coarse on deep uniform waters.
The mesh covers all the eastern coast until Sydney with the open boundary in the East following a kind of isobath at 4500-4800 meters deep. In the North, the choice has been

[7] https://www.ncdc.noaa.gov/

made to take only half of the GBR. We can indeed assume that if there are larvae exchanges between the GBR reefs and outer reefs, this concerns the southern reefs of the GBR. Indeed it is difficult to imagine larvae floating further than 200km and so the northern boundary at 19° S is pushed north enough to observe these hypothetical exchanges (see figure 2.10).

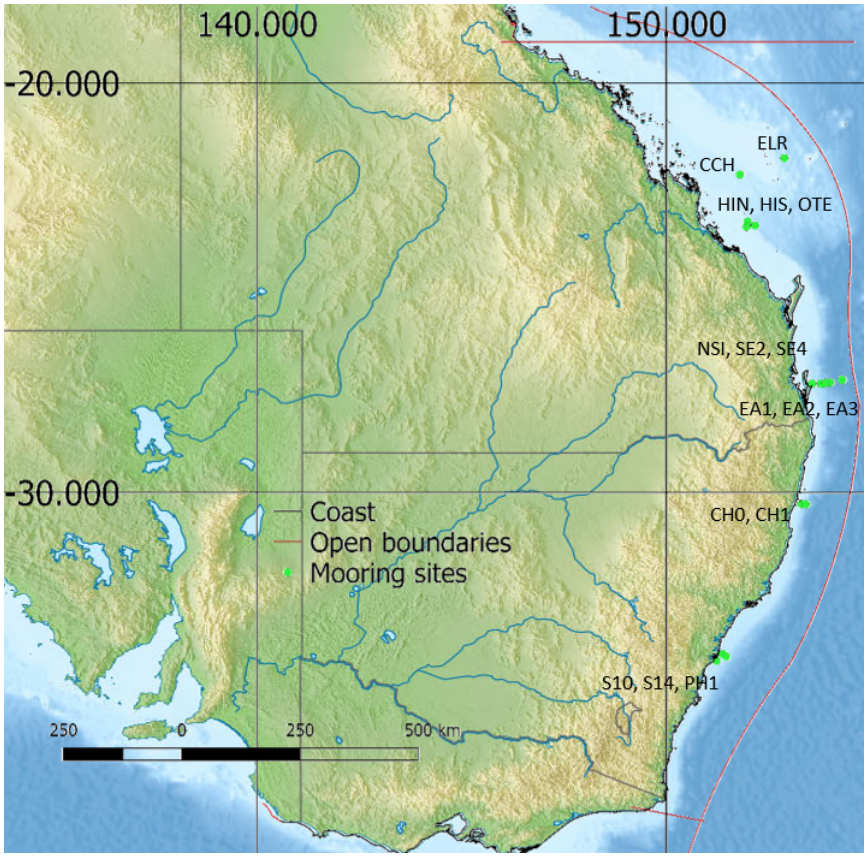

Figure 2.10: The domain of study with the validation points.

Since it has been decided to increase the resolution on reefs and next to the coasts, it seemed acceptable not to take into account the water depth. In our domain, we observe shallow waters where there are reefs and vice versa, which leaves the bigger meshes elements for deep water regions.

In order to take into account the coastal parameters to define the mesh size $\Delta_c(d)$, we use the distance to the nearest coastline d.

$$\Delta_c(d) = \begin{cases} l_0 & \text{if } d \leq d_0, \\ l_0 \left(\frac{d_1 - d}{d_1 - d_0}\right) + l_1 \left(\frac{d - d_0}{d_1 - d_0}\right) & \text{if } d_0 \leq d \leq d_1, \\ l_1 & \text{otherwise.} \end{cases} \tag{2.6}$$

where $l_0 = 500m$, $l_1 = 10km$, $d_0 = 15km$ and $d_1 = 50km$.

We use the same process to take into account the distance to reefs, with d being the distance to the nearest reef.

The local mesh size Δ is then the minimum of $\Delta_c(d)$ and $\Delta_r(d)$. The mesh thereby constructed is showed on figure 2.11. Such a mesh has about $7.35 \cdot 10^5$ elements.

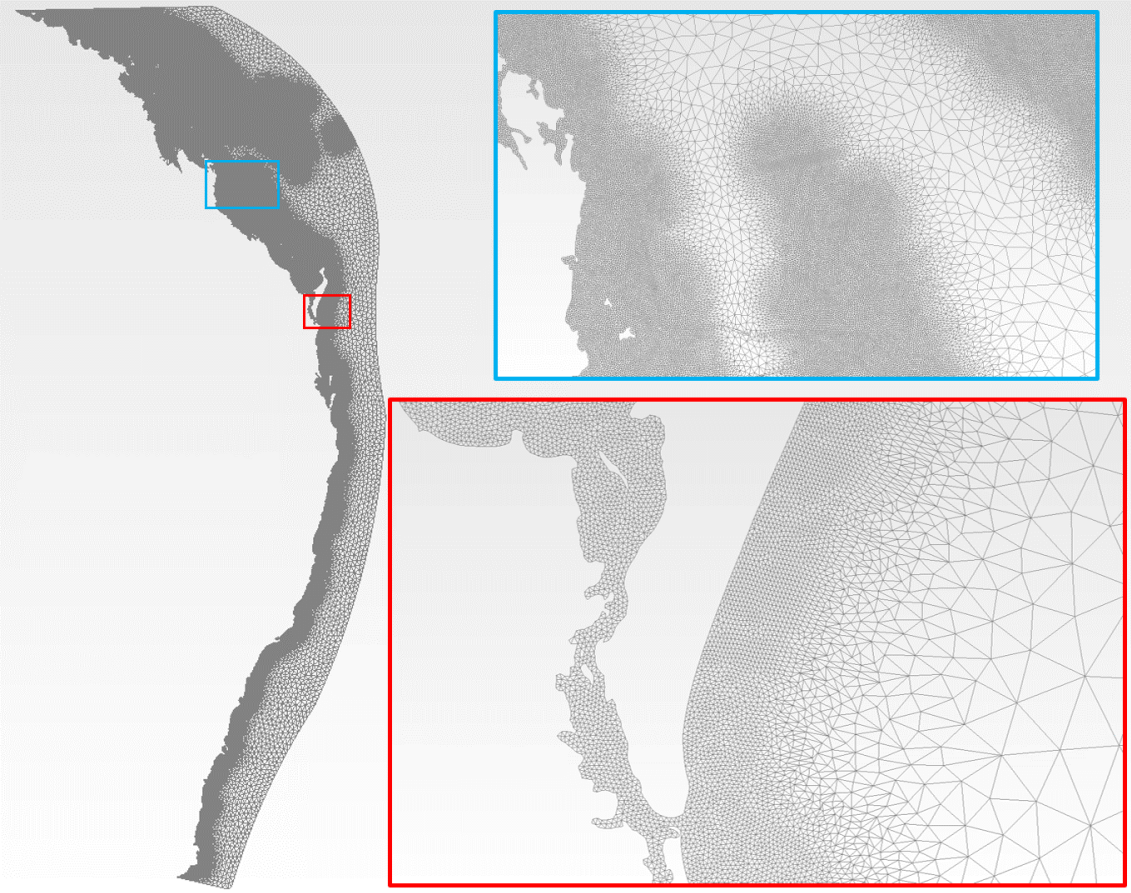

Figure 2.11: The constructed mesh, from 500m resolution around reefs and coast to 10km

2.4 Forcings

In order to obtain our realistic model, we need to apply three external forcings: winds, tides and large scale water circulation due to the East Australian Current. We will chose a period covering the spawning of coral larvae in Australia. The period chosen is from November 30, 2012 to February 28, 2013. The spawning happened at the beginning of December, letting our model some time to adjust itself and being long enough to follow the full larvae displacements.

As said in section 2.2, we get our wind speeds (10 meters above the sea) dataset from the model CFSv2. First we have to interpolate this dataset (given on a regular grid) on

our unstructured mesh, then it can be integrated in equation 2.2.

We extract the tidal forcing from the OSU TOPEX/Poseidon Global Inverse Solution TPXO dataset [Egbert and Erofeeva , 2002], which gives the amplitude and phase of the main tidal components on a 0.25° resolution global grid. These components can then be reconstructed into tidal elevation and velocity that are imposed on open boundaries.

To introduce large scale water circulation in our model, we have to impose data collected from a global hydrodynamic model on the boundaries of the mesh. So we took currents data from HYCOM. As said above, HYCOM is a 3D model on a 1/25° grid. We have to flatten the data by depth-averaging the velocities provided by HYCOM. Once we have summed HYCOM elevation and velocities with TPXO tidal elevation and velocities, we can impose the results on the red open boundaries of figure 2.10.

From the description of HYCOM given at section 2.1, we can say that it is more suitable to model physical processes in deep water than our 2D version of SLIM. That is why a relaxation term is added to the model. We aim to keep SLIM's modeled velocities close to the HYCOM ones on deep and far off-shore regions mainly. The relaxation is then at its maximum on the open boundaries in deep ocean. The global circulation forcing $\mathbf{F}_{gc}$ is defined as follows:

$$\mathbf{F}_{gc} = \gamma(\mathbf{u}_* - \mathbf{u}) \tag{2.7}$$

where $\mathbf{u}_*$ is the depth-averaged velocity obtained from the addition of HYCOM's velocities with the downloaded tides' velocities and $\gamma = \tau^{-1}$ is the inverse of the relaxation time τ.

γ is defined as follows:

$$\gamma(d,h) = \gamma_{coast}(d) + \gamma_{depth}(h) \tag{2.8}$$

with

$$\gamma_{coast}(d) = \begin{cases} 10^{-5}\left(\frac{10^5-d}{10^5}\right) & \text{if } d \leq 10^5 m, \\ 0 & \text{if } d > 10^5 m. \end{cases} \tag{2.9}$$

and

$$\gamma_{depth}(h) = \begin{cases} 0 & \text{if } h \leq 50m, \\ h \cdot 10^{-7} & \text{if } 50m \leq h \leq 300m, \\ 3 \cdot 10^{-5} & \text{if } d > 300m. \end{cases} \tag{2.10}$$

The value of γ on our domain is shown in figure 2.12.

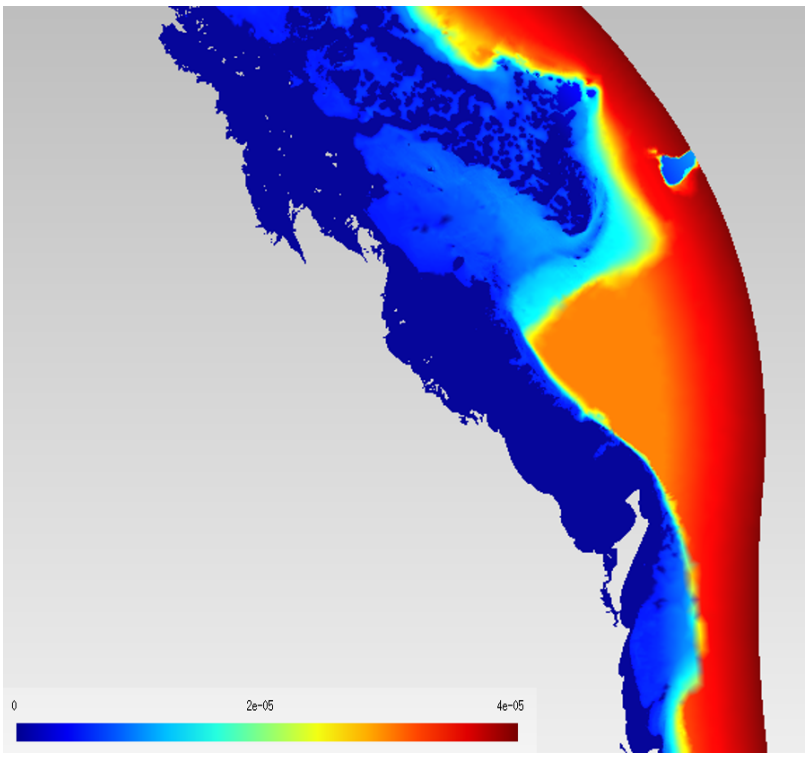

Figure 2.12: Value of γ. There is no relaxation toward HYCOM where $\gamma = 0$.

2.5 Validation

Several mooring stations from the Integrated Marine Observing System (IMOS)[8] are located in our domain. A part of them are placed in the GBR and some others are further south (see figure 2.10).

All the data collections that they gather are available online on the portal AODN (Open Access to Ocean Data), including "Current velocity time-series" collected from moorings deployed by the Australian National Mooring Network (ANMN). The current data were obtained from Acoustic Doppler Current Profilers. This gives us quite fairly thorough data to validate the velocities computed by our model.

We also need to validate the sea-surface height η. This variable was complicated to validate due to the poor amount of precise data available. If we put aside the satellite datasets (which are extremely coarse), there remains only the "depth" data collected by the same mooring stations mentioned above. The relevance of this variable will be discussed

[8] http://imos.org.au/

#	code	Name	**u** data	η data
1	ELR	Elusive Reefs	$\surd$	$\times$
2	CCH	Capricorn Channel	$\surd$	$\surd$
3	HIN	Heron Island North	$\times$	$\times$
4	HIS	Heron Island South	$\times$	$\times$
5	OTE	One Tree East	$\surd$	$\surd$
6	EA1	East Australian Current 1	$\surd$	$\times$
7	EA2	East Australian Current 2	$\surd$	$\times$
8	EA3	East Australian Current 3	$\surd$	$\times$
9	SE2	South East Queensland 200	$\surd$	$\times$
10	SE4	South East Queensland 400	$\surd$	$\times$
11	NSI	North Stradbroke Island	$\surd$	$\surd$
12	CH0	Coffs Harbour 070	$\times$	$\times$
13	CH1	Coffs Harbour 100	$\times$	$\times$
14	S10	Sydney 100	$\times$	$\times$
15	S14	Sydney 140	$\times$	$\times$
16	PH1	Port Hacking 100	$\surd$	$\surd$

Table 2.1: Summary table of the mooring stations and information about the data availability for each corresponding to our period (30/11/2012 to 28/02/2013).

below.

First we compare the velocities computed by our model to mooring data and the results of the model HYCOM combined with TPXO (see figure 2.13, 2.14 and 2.15). The mooring data are taken when it was available but it appeared that not all the chosen stations were collecting data at our precise period. The results for the stations without data are nevertheless computed, to be compared to the superposition of HYCOM and TPXO 's results.

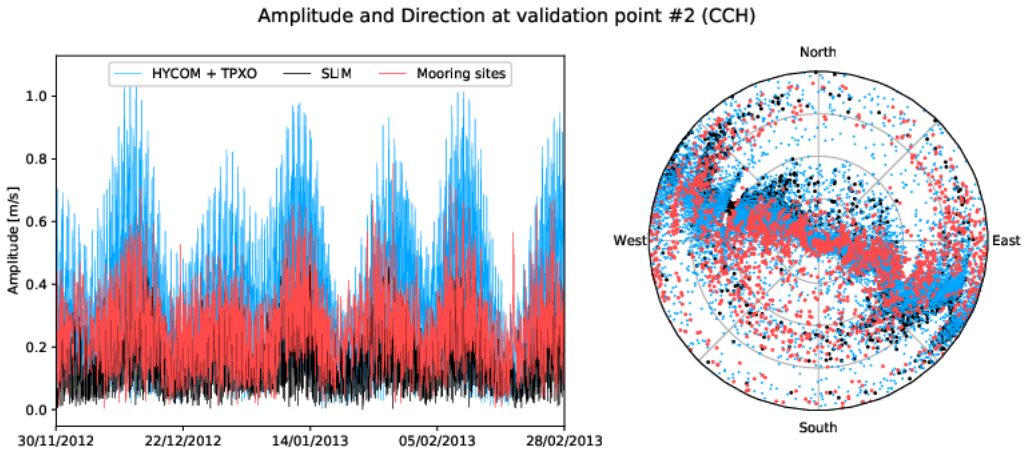

Figure 2.13: SLIM computed a good approximation in terms of amplitude. The direction is similar to HYCOM's even if the direction measured by the mooring station is very shifting.

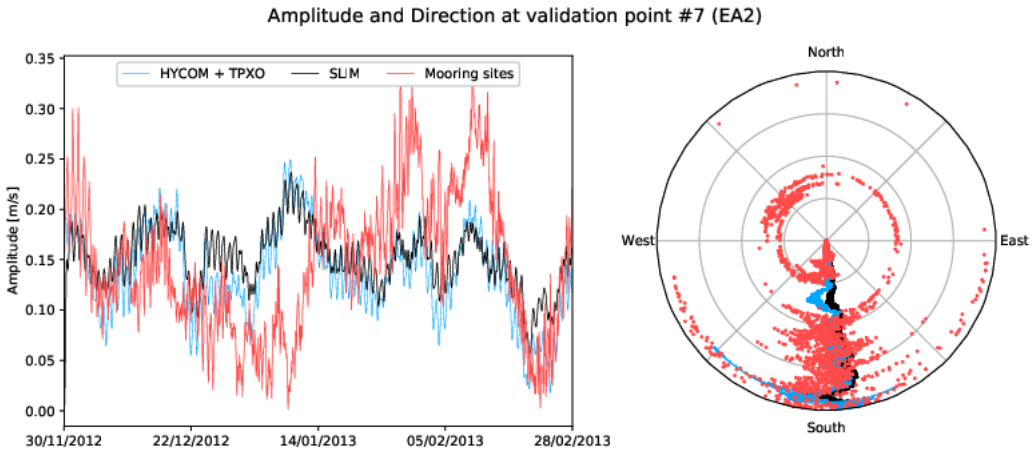

Figure 2.14: On this point the relaxation towards HYCOM is significant. This implies similar amplitudes and directions for HYCOM + TPXO and SLIM. The data of the mooring sites proves that the models are pretty accurate.

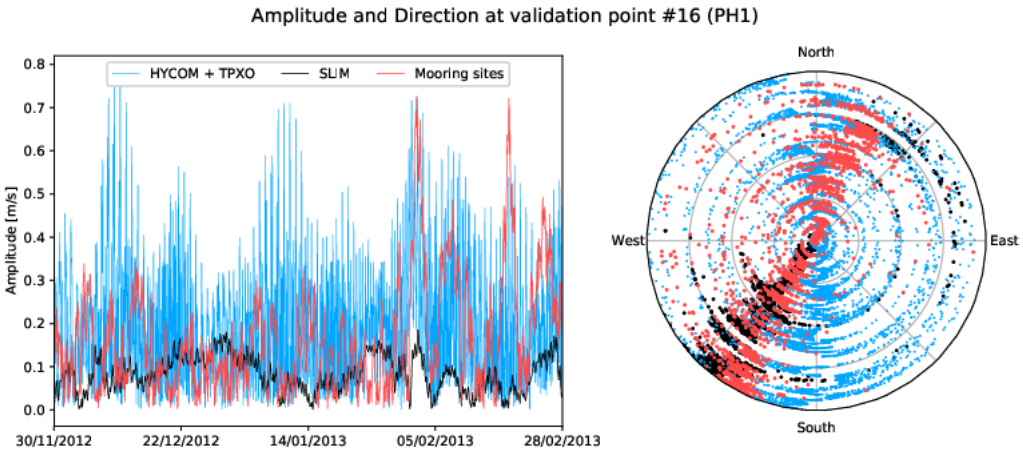

Figure 2.15: This point next to Sydney and not far from the coast proves the advantage of SLIM over HYCOM in this type of region. The amplitude and the direction are good.

Then we compare the water elevation to the variable "depth" that we have (see figure 2.16 and 2.17). We will also confront our results with the superposition mentioned above. Even though HYCOM is also a model and is therefore not immune to errors, it is widely used and has been extensively validated, which is why we chose to rely on it when no mooring data was available.

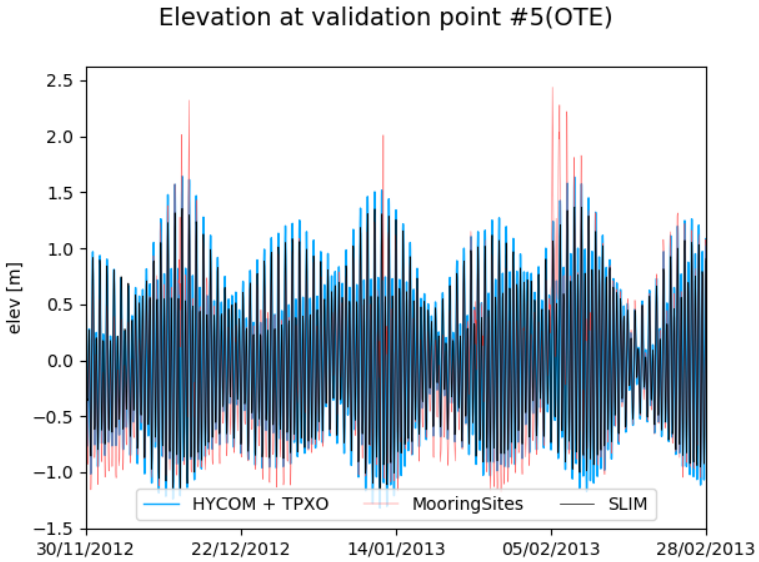

Figure 2.16: This point located in the GBR is one of the few stations that provided coherent values for η. Not all the peaks are well fitted by SLIM but the general pattern looks good.

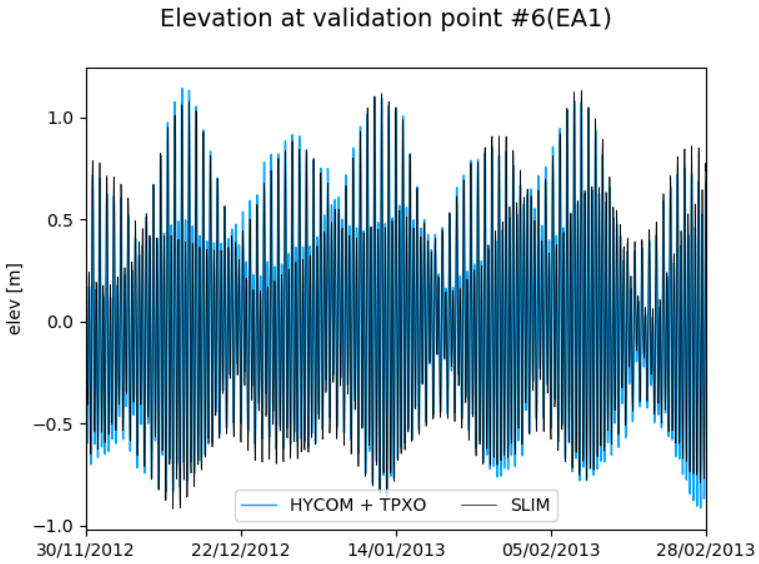

Figure 2.17: This point is far from the coast, so it is not surprising that SLIM is close to HYCOM since the forcing on the open boundary is close.

These results are shown here because of their relevance, the rest of the results are made available in the Appendices.

2.6 Limitations

As said before, we can indeed wonder about the reliability of the variable "depth". The comment provided by the ANMN specify: "Depth computed from latitude and relative pressure measurements". This is thus a computed data (unlike buoy data), which makes it questionable. And in our case, major problems of incoherence (see figure 2.18) were found for 12 out of the 16 datasets that we have. On most of the mooring sites' datasets, the SSH does not oscillate around an almost constant value but constantly decreases (in the case presented in figure 2.18, on other points it constantly decreases). The Δh then created can reach tens of meters.

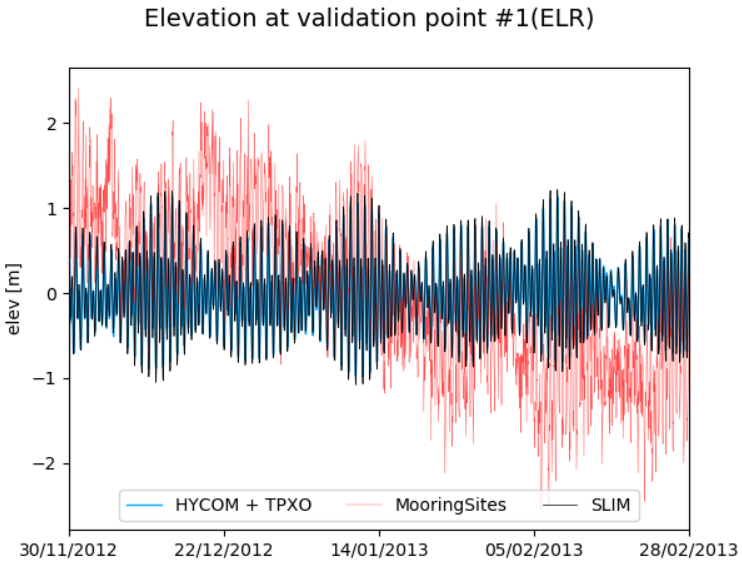

Figure 2.18: The illustration of the incoherent variable "depth". During the 3 months η does not stop decreasing. On other datasets, this difference is in tens of meters.

Furthermore the choice of a 2D model has already been discussed; vertical dynamics of the ocean can not be well modelled. But it also brings another question during the validation. The current velocities are available over the entire height of the water column. Do we have to take the mean on the entire height since we flattened the HYCOM data this way ? Or do we have to take the values on the lesser deep measures since the larvae disperse close to the surface ? In this study we chose the first way, but it could still be of course debatable.

Our main problem is the lack of mooring data. We will not be able to go further than a graphical analysis of our results since the comparison data were unreliable for the most part. Indeed harmonic analysis such as the TAPPY (Tidal Analysis Program in PYthon) does not make sense since it analyzes the elevation variations (amplitudes and phases).

3 Modelling larval dispersal

Now that we have a hydrodynamic model, we can model the larval dispersal. Since our goal is to study the connectivity between reefs, we will have to simulate the release, the dispersal and the settlement of the larvae. We assume these larvae to be passively transported by the ocean currents, which allows us to define these larvae with few parameters.

3.1 Lagrangian particle tracker

In this study we will use the same method used in other studies to model the transport of particles [C. Thomas , 2015; Bechet and Verstraeten , 2018]. We will then use a random walk formulation of the 2D advection-diffusion equation to represent turbulence [Spagnol et al. , 2002; Hunter, Craig, and Phillips , 1993]. The Lagrangian algorithm in its discretised form is the following:

$$\mathbf{x}_{n+1} = \mathbf{x}_n + \mathbf{v}_n \Delta t + \frac{\mathbf{R}_n}{\sqrt{r}} \sqrt{2K\Delta t} \tag{3.11}$$

with

$$\mathbf{v}_n = \left(\mathbf{u} + \frac{K}{H} \nabla H + \nabla K \right) |_{\mathbf{x}_n} \tag{3.12}$$

where $\mathbf{x}_n$ and $\mathbf{x}_{n+1}$ are the particles positions at time iterations n and $n+1$ respectively, Δt is the time difference between iterations, K is the horizontal diffusivity coefficient, $\mathbf{u} = \mathbf{u}(x,t)$ is the instantaneous depth-averaged horizontal water velocity modeled with SLIM, H is the water column depth, and $\mathbf{R}_n$ is a two-dimensional vector of random numbers with a mean of zero and a variance of $r \equiv < R^2 >$ ($\frac{\mathbf{R}_n}{\sqrt{r}}$ is a vector of random numbers with unit variance).

Equation 3.11 can be split in two terms. As a matter of fact, if the last term is removed, we find the obvious deterministic part $\mathbf{x}_{n+1} = \mathbf{x}_n + \mathbf{v}_n \Delta t$, where $\mathbf{v}_n$ is defined in equation 3.12. But as this equation is called a random walk formulation, it has to contain a stochastic term. It allows us to take into account the effect of random sub-grid scale turbulence. Its effect is increased for high diffusivity coefficient regions. This term also wraps the uncertainties of life. Corals don't escape nature's laws, their lives depend on random events and that is why the same Lagrangian Particle Tracker (LPT) model is run 10 times, so that the random vector $\mathbf{R}_n$ changes each time.

We will define the horizontal diffusivity coefficient K the same way [de Brye et al. , 2011] did, who were themselves inspired by [Okubo , 1971].

$$K = \alpha \Delta^{1.15} [m^2 s] \tag{3.13}$$

where Δ is still the local element size of the mesh. This dependency on Δ is interesting for it supposes that the larger the mesh elements are, the more unresolved water flows will be in it. [Andutta, Ridd, and Wolanski , 2011] calibrated α for coastal waters in the GBR, we will thus also take $\alpha = 0.041 m^{0.85} s^{-1}$.

As said in section 2.1, the LPT is a module of SLIM. The results of the hydrodynamic model (H and $\mathbf{u}$) become the LPT's input. Time parameters are the same as for the hydrodynamic model: the time step $\Delta t = 900s$ and the outputs are recorded every hour.

3.2 Acropora Millepora

This study doesn't claim to analyse biologic topics; up to here we focused on geophysical processes, simplifying as much as possible the biological aspects. However, the particle tracker of SLIM allows the user to set some biological parameters to define the particle. We will then compress all these aspects of the larvae in 3 parameters: competence, settlement and mortality.

The species chosen for this study is *Acropora Millepora*, which is a common species growing in shallow waters. These corals are widely distributed in tropical and subtropical waters, which makes them a good species to work with in our case.

Figure 3.19: Acropora Millepora. Source figure: *Reef builders*, May 2017

Let's begin with competence. We need to set the ability of a larva to settle onto a reef. The larva is not immediately able to settle, it needs a latency period. According to [Figueiredo, Baird, and Connolly , 2013] (based on [Connolly and Baird , 2010]), we

can set the latency period to 3.526 for A. Millepora. After this period, the larvae have an acquisition rate constant of 0.348 day^{-1}. In this study the loss of competency is not modeled.

When a larva is competent, it can lose its buoyancy, sink down and attach to a reef. This process is the settlement. SLIM allows to select reefs on which larvae can not settle, depending on their depth. In our model, we made the assumption that if a larva is competent and passes over a reef, it settles onto it automatically. Such an event causes the LPT model to remove the larva and to record the settlement in the connectivity matrix.

The last implemented biological parameter is the mortality rate of the larvae. This rate is constant and is set to 0.054 day^{-1} [Figueiredo et al. , 2013].

The spawning location follows the reefs location. That implies the assumption that all the colored areas on the map are covered with reefs and that A. Millepora fully covers these areas (regardless of the other species). This is surely far from reality, but since no reliable data about the proportion of each reef covered by A. Millepora is available, we will continue with these assumptions.

We interpolated the reef map on our mesh and gave to each isolated reef thereby created an index (see figure 3.20). This operation produced 1329 reefs on our mesh.

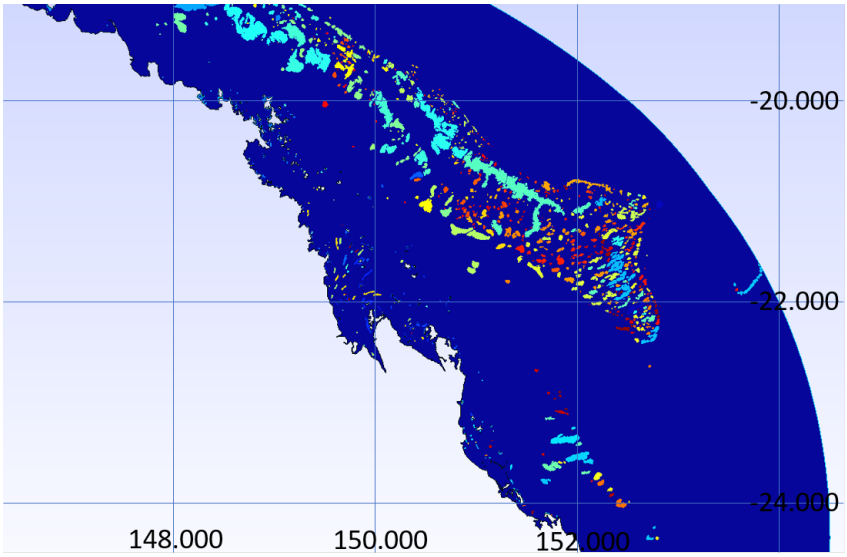

Figure 3.20: The reef map is interpolated on the mesh, each reef is identified with an index from 1 to 1329. On this figure, the indexes are represented with colors.

The initial concentration of particles is fixed at 50 $larvae/km^2$.

In 2012, the spawning of Millepora larvae took place during the night between December 4 and December 5. Since we had to run the model 10 times to randomize the dispersal (see section 3.1), we chose to spread the spawning along the night between 9pm to 3am. The model is run 30 days after the spawning. At that time only $4,6\%$ of the larvae are

still alive and competent under the conditions we established above.

Following this procedure, we get 77489 "habitat elements" (i.e. the mesh elements that are considered as reefs after the interpolation). They form 1379 distinct habitats on which a total of 1.2410^6 (the exact number varies slightly following the different runs) are seeded. The graph in figure 3.21 is built from the results of a run and summarizes the evolution of the population.

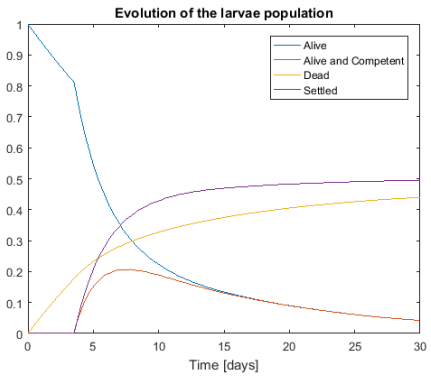

Figure 3.21: This graph follows the evolution of the larval population and details the different possible states of the particles in the model. We can observe the latency period before acquiring competence.

A slight overview of the larval dispersal simulation on the GBR is shown in figure 3.22; snapshots are taken before the release and after 15 and 30 days of drifting.

The same approach is followed for a small part of the southern reefs, with different time steps (see figure 3.23).

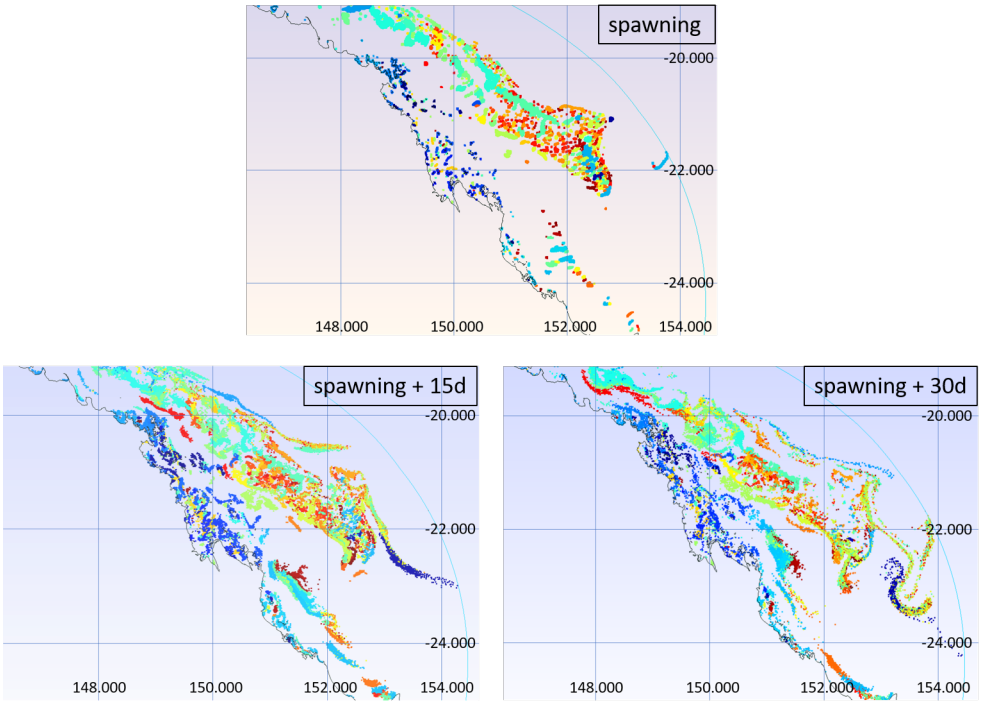

Figure 3.22: The larval dispersal in the GBR after 15 and 30 days.

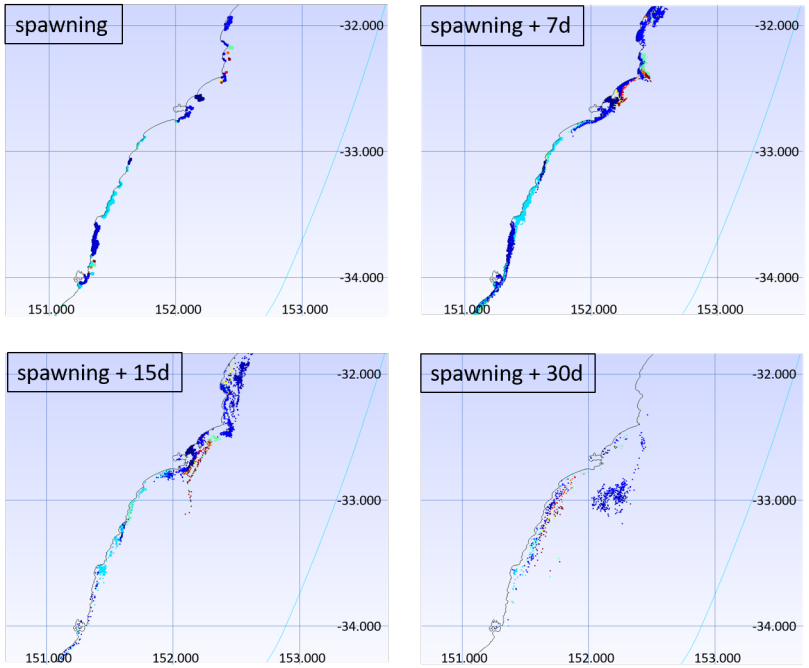

Figure 3.23: The larval dispersal on southern reefs after 15 and 30 days.

3.3 Discussion

We took $\Delta t = 900s$. Since we use a Lagrangian Particle Tracker, the path of the particle is computed from the velocity on the starting point. That means that a particle initially pushed by a current of 1m/s (which can be found in our domain) will travel 900m before the next iteration, which is larger than the smaller mesh elements (500m). This value of Δt is nevertheless not decreased to keep a reasonable computational cost.

As said above, we made the assumption that all the regions given in the shapefile layers are covered by A. Millepora. This can't be improved unless more precise data is constructed (geographically and with species distinction). This comment is supported by the fact that the temperate reefs are kelp-dominated. The areas given in the maps are therefore not at exclusively covered by A. Millepora. A better, actual percentage of coral cover for each coral species is needed to give more validity to these results.

The computational cost that prevented us from taking a smaller Δt also limited us regarding the minimum mesh size. The reef maps we used have a higher resolution than our mesh. This implies a loss of information during the interpolation. What is represented by a single reef in our model can in fact hide reef communities where the reefs are separated by a few hundred meters, as it is shown in figure 3.24. This fact should not be forgotten during the connectivity analysis.

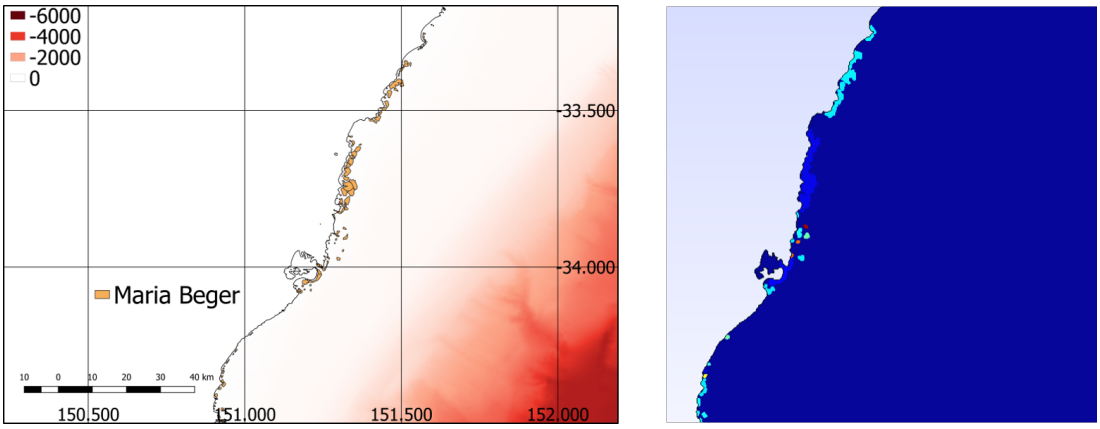

Figure 3.24: These 2 communities extends on almost 20 km each and are composed of a dozen of distinct reefs and yet they are represented as a unique reef in our model.

4 Graph theory tools

The results discussed above allow to draw the graph in figure 4.25. Every point is a reef while every line represents an exchange of larvae between two reefs. The first observation we make is that the GBR and the southern reefs are well separated; they do not exchange larvae.

This graph only gives a small glimpse of the connectivity; we have to analyse deeper the data that we have with a selection of graph analysis tools.

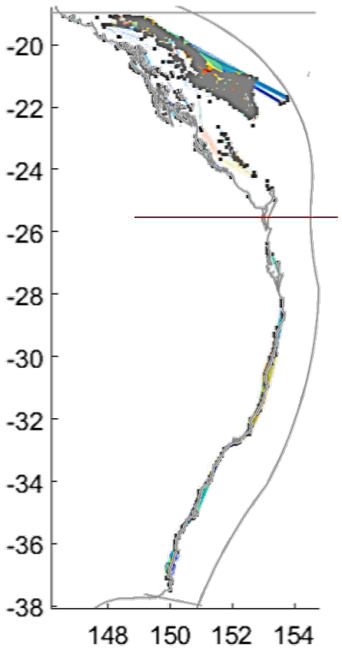

Figure 4.25: The graph of connectivity, where the points are the reefs and the lines are the exchanges of larvae. It truly forms two separate graphs from either side of the red line.

4.1 Connectivity matrix

We now have to extract information from the dispersal simulation. The previous step fills a connectivity matrix C. It works as a basic adjacency matrix describing a directed graph. Each element C_{ij} is the number of larvae released by the reef i that settled onto the reef j.

We will also use two other outputs S and X. S_i is the total number of larvae released by the reef i during the simulation while X contains the coordinates of each reef.

Since the dispersal has been modelled with 1329 reefs (as said in section 3.2), the matrix thereby created is thus very large (1329×1329). Collecting information from it is not an easy task; that is why it will be done with predefined tools described in this section. These tools have already been used in other studies about coral connectivity [Bechet and Verstraeten , 2018; Frys , 2018; Hanert et al. , 2012].

As mentioned earlier, 10 runs of the LPT model are executed. The resulting matrix C and seeding vector S are different for each run (due to the stochastic part of the equation 3.11). The 10 matrices and vectors are added in order to avoid giving too much importance to a very unusual result.

4.2 Connectivity indices

The following indices have been selected to describe and analyze the regions of interest to the best of our ability. The definition of these indices is outlined below.

4.2.1 Local retention

This index is the proportion of larvae initially seeded by a reef that settle on the same reef.

$$LR_i = \frac{C_{ii}}{S_i} \tag{4.14}$$

It can be interpreted as the selfishness of the reef, its ability to keep the larvae it spawned for itself. This capacity is especially useful when the reef is isolated, when it does not receive many larvae from other reefs.

4.2.2 Self recruitment

This index is the proportion of larvae settled on a reef which were released over the same reef.

$$SR_i = \frac{C_{ii}}{\sum_j C_{ji}} \tag{4.15}$$

The difference with the previous index lies in the fact that this time we divide the larvae released by a reef seeding on the same reef by the total number of larvae that settled onto this reef. A reef with a high SR is a reef that needs less larvae from others than a reef with a low LR, which is more isolated.

4.2.3 Proportion settled

This index is defined as the proportion of larvae released by a reef that settle on other reefs.

$$P_{settled,i} = \frac{\sum_{j \neq i} C_{ij}}{S_i} \tag{4.16}$$

Since the local retention is not taken into account, it allows to represent how much a reef is a source for other reefs.

4.2.4 Proportion lost

This index is defined as the proportion of larvae released by a reef that never settle on any reef (including itself).

$$P_{lost,i} = \frac{S_i - \sum_{j} C_{ij}}{S_i} = \frac{S_i - \sum_{j \neq i} C_{ij} - C_{ii}}{S_i} = 1 - P_{settled,i} - LR_i \tag{4.17}$$

This index completes $P_{settled,i}$ and LR_i since their total equals 1.

4.2.5 Weighted connectivity length

This index is the average distance traveled by the larvae released from a reef who end up settling on a reef (including itself).

$$WCL_i = \frac{\sum_{j} C_{ij} L_{ij}}{\sum_{j} C_{ij}} \tag{4.18}$$

where L_{ij} is the radial distance between the reefs i and j, computed using the coordinates of the reefs stored in X.

This index uses the particles, not the reefs. This way the connectivity length is weighted by the strength of the links between reefs.

4.2.6 PageRank

The objective here is to rank the reefs the same way Google did it initially with websites [Page, Brin, Motwani, and Winograd , 1999]. PageRank is a recursive algorithm that gives a numerical weighting to each page to measure its relative importance. This weighting is greater if the links to the page are numerous and if these links come from pages that are themselves well ranked. Indeed a forwarding link has more value if it is itself pointed at by a large number of pages.

This principle will be used to identify the most important sinks and sources. The sinks will be determined with the quality and the quantity of the incoming connections (with the

index Incoming PageRank π^{in}) while the outcoming connections will be used to determine the sources (with the index Outcoming PageRank π^{out}). The Matlab function "centrality"[9] will be used in "pagerank" mode to apply these principles. The sum of all the PageRank indices over the domain $\sum \pi^{in} = \sum \pi^{out} = 1$.

4.3 Protection and restoration indices

The previous indices are used as tools to extract information about the reefs. It is interesting to transform and use this information to have clues about the coral reef management. These clues on where and how to act can be extremely useful for the people already working on sustaining coral reefs.

4.3.1 PageRank protection index

The reefs that need protection are the ones useful to their community but that do not receive as much from the others. In other words they are good exporters but poor importers. The PageRank protection index is constructed as follows:

$$\pi_i^{out-in} = \frac{\pi_i^{out} - \pi_i^{in}}{\pi_i^{out} + \pi_i^{in}} \tag{4.19}$$

π^{out-in} is defined as the difference between π^{out} and π^{in} normalized by their sum. Its value is therefore in the interval [-1;1]. Reefs with a π^{out-in} close to 1 are those who need protection in priority. On the contrary, those with a value close to -1 are reefs that import well and export little. They are already resilient, sort of dead ends of the graph.

4.3.2 PageRank restoration index

We want the reefs we restore to be useful both to the community and to themselves. The PageRank restoration index is then constructed as follows:

$$\pi_i^{out\times in} = \pi_i^{out} \times \pi_i^{in} \tag{4.20}$$

The index thereby created is high if the reef is both a good source and sink.

4.4 Communities and reef clusters identification

The connectivity analysis can be continued with the identification of reef clusters. In this study we will use the "strongly connected components" (SCC) method.

[9]The description of the matlab function is available at https://www.mathworks.com/help/matlab/ref/graph.centrality.html

This method is rather simple, it groups all the reefs that are connected in both directions. This connection can be indirect, it can pass through a third reef (or more). If two reefs A and B are in the same cluster, it means that there is a way from A to B and a way from B to A (this way can be indirect).

5 Connectivity analysis

5.1 Connectivity matrix

The connectivity matrix obtained after 10 runs is shown in figure 5.26. However there is not much to be learned from it in this form and that is why we sorted it according to the reefs' latitudes. New indices have been attributed to each reef, the most northern reef received the 1 while the most southern got the 1379.

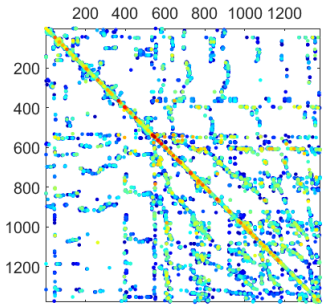

Figure 5.26: The initial connectivity matrix.

The figure 5.27 is a bit more interesting since we can clearly see the separation between the GBR latitudes and the subtropical ones. The upper part is wide while the lower part is close to the diagonal. The red line drawn on figure 4.25 is also visible. It corresponds to a tightening of the matrix on an element of the diagonal.

We have actually divided this matrix and kept the lower part since the subpart containing the last 252 rows and columns is the one concerning the reefs south to the GBR. This sub-matrix will be rather useful to obtain results that are specific to this region.

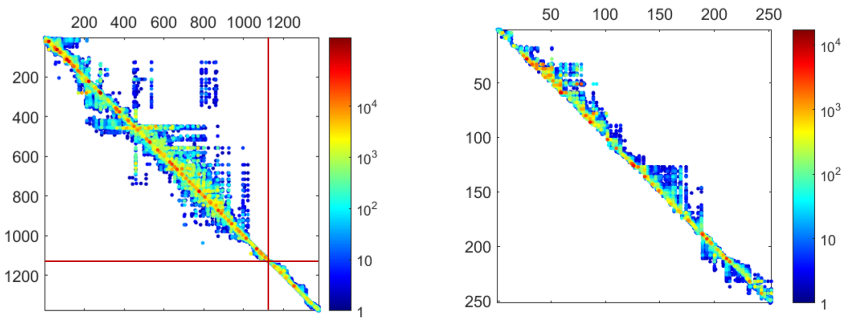

Figure 5.27: The sorted connectivity matrices of the whole domain and of the southern part.

5.2 Connectivity indices

Now that the tools have been defined, this section presents the resulting indices computed with our case.

5.2.1 Local retention

The reefs with the highest LR are the ones located in the inner part of the GBR (see figure 5.28). The outermost reefs of the GBR see their larvae being swept away faster (before acquiring their competence) and out of reach.

in the southern part the LR is mostly dependent on the influence of the EAC. The more the effect of the EAC is felt, the faster the larvae drift south (or/and into the deep water). The reefs with the highest LR are those whose larvae remain the longest (until acquiring competence) under the dominant influence of the tide.

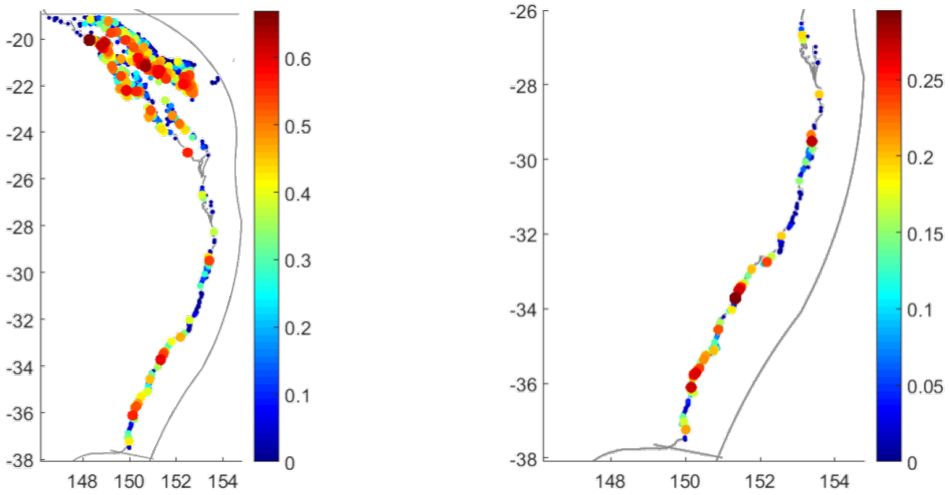

Figure 5.28: Local retention in the whole domain and in the southern part.

5.2.2 Self recruitment

A large number of the GBR's reefs has a high SR (see figure 5.29). There are two major explanations for this: the size of the reef and the time to acquire competence.

Some large reefs enjoy less contribution from smaller reefs nearby since the number of larvae seeded that settle on the same reef is divided by the total number of seeded larvae on this reef. As we compare numbers and as the number of seeded particles depends on the surface of the reef, the size of the reef influences SR.

With little residual current, the larvae are likely to be close to where they were released after the time required to make them competent. As said in section 3.2, the larvae settle on the first reef it passes over. This means that if the larvae do not drift "enough" before acquiring competence they settle on the reef from which they were released.

In the southern area the more isolated reefs (the ones with higher SR) are more frequent. There are some groups consisting of a few reefs; those outside these groups are more autonomous (because more isolated).

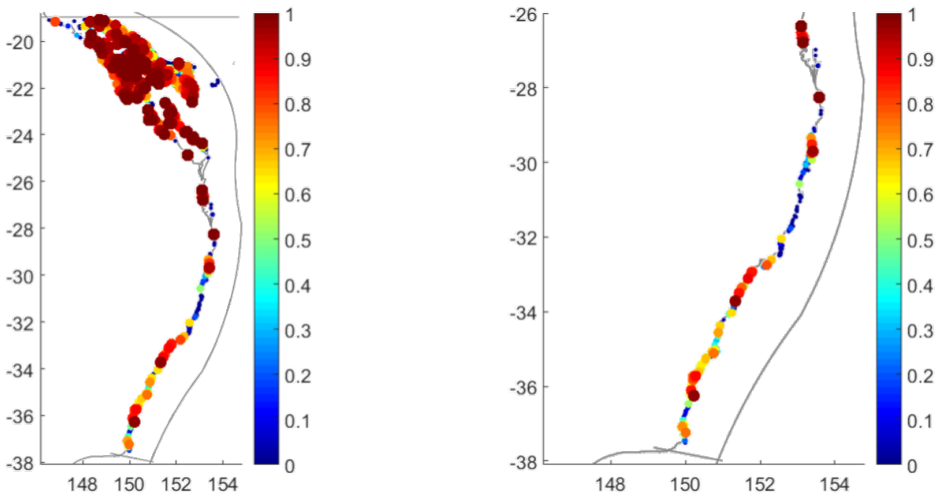

Figure 5.29: Self recruitment in the whole domain and in the southern part.

5.2.3 Proportion settled

For this index as well as for the following, the GBR division distorts the results in the northernmost region (see figure 5.30). A good part of the seeded larvae do not settle when they could have done it on more northerly reefs. This increases the value of P_{lost} and decreases $P_{settled}$ of these northern reefs.

We can still notice good values for reefs on the regions at the border of the GBR. They are exposed to a current a bit stronger than in the inner region, allowing them to share their larvae with nearby reefs.

In the subtropical part, the reefs with high $P_{settled}$ are among the less isolated. The reefs located between 29 and 32°S are under the influence of the EAC. The latter acts as a conveyor belt, pushing the larvae south along the coast. Under these latitudes specifically, the EAC seems to run alongside the coast, allowing these reefs to provide more larvae to southern reefs.

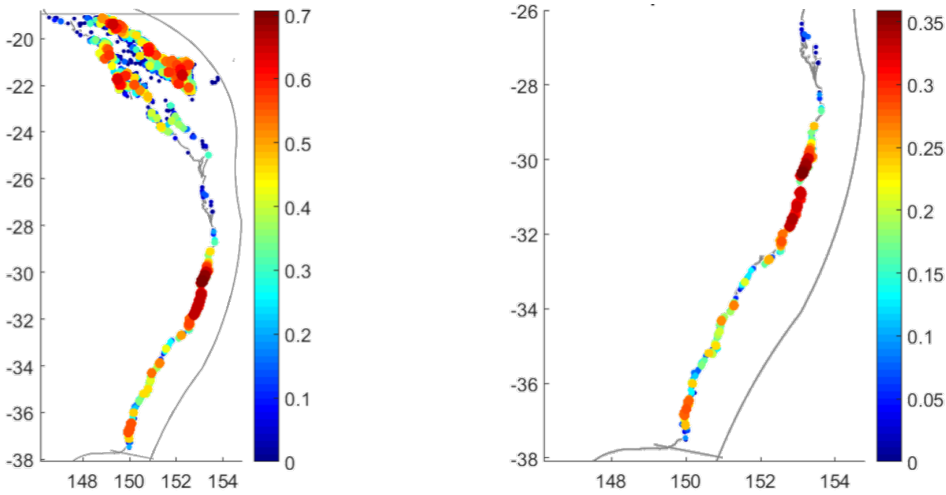

Figure 5.30: $P_{settled}$ in the whole domain and in the southern part.

5.2.4 Proportion lost

A northward residual current acts on the inner part of the GBR. The larvae transported leave the domain and will never be counted in the settled larvae, increasing the P_{lost} of their respective reefs (see figure 5.31).

The subtropical reefs work in communities; the small groups consisting of a few reefs (still according to the given files) are separated from each other by a greater distance. Apart from the region between 29 and 32°S, a significant part of the larvae is then lost (even more so for the reefs at the south of these groups).

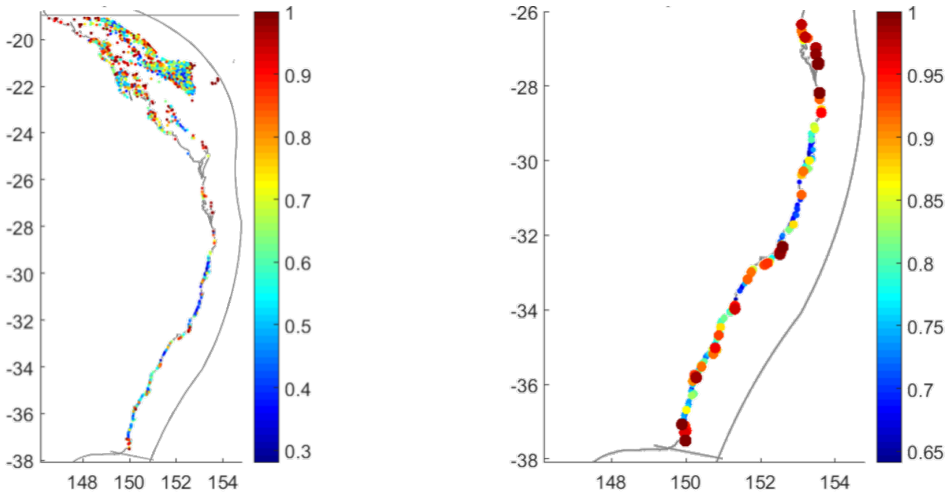

Figure 5.31: P_{lost} in the whole domain and in the southern part. The size of the points in the graph of the whole domain does not follow the index value due to visibility concerns.

5.2.5 Weighted connectivity length

Apart from the few reefs that have a WCL over 200km, the WCL is relatively short (see figure 5.32). This is due to the short period needed by A. Millepora to acquire its competence coupled with the assumption that the larvae settle on the first reef they pass on (once the competency is acquired).

In the GBR, unless they have been carried far enough before acquiring competence, which concerns mainly outer eastern reefs, the larvae settle rather quickly after acquiring competence due to the high density of reefs.

The larvae released by subtropical reefs travel more kilometers but the ones who travel the most are less likely to settle later (carried toward the deep ocean). The main part of larvae that settle are the ones that do it on their own reefs or on reefs of the same small group. Once again, the reefs at 30-32°S are "the exception", benefiting from the EAC along the coast over several tens of kilometers.

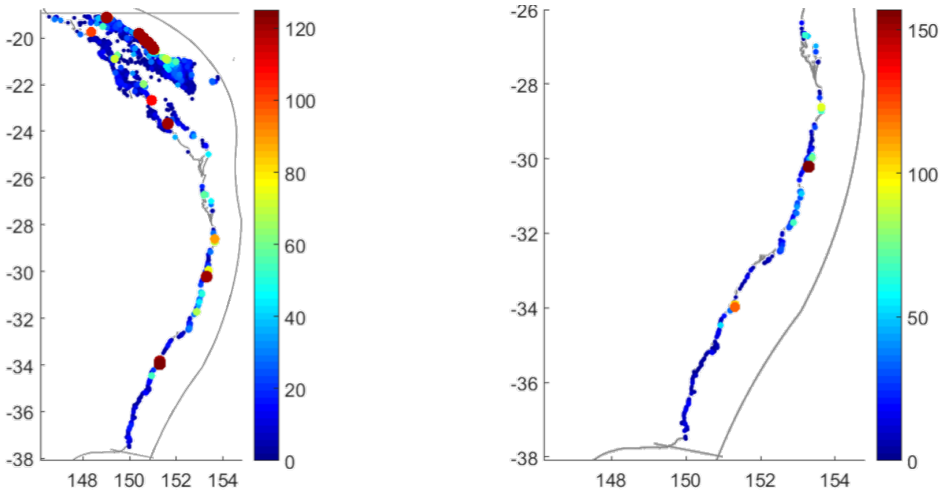

Figure 5.32: The WCL in the whole domain and in the southern part. The upper limit of WCL in the graph of the whole domain has been limited to 120km due to visibility concerns (3 reefs in the GBR have values above 200km).

5.2.6 PageRank

The PageRank indices can not be seriously taken into account since the "hyperlink set" is not complete. Indeed, since we split the GBR, we missed some of the elements composing the set of reefs. The result for π^{in} and π^{out} on the whole domain are still shown in figure 5.33 and 5.34.

In the southern part, the reefs south of the zone 30-32°S have a better π^{in} since they represent the end of an important zone of exchanges. In the south near Sydney there is also a medium-sized community and some reefs of this community also have a good π^{in} (see figure 5.33).

The reefs with the better π^{out} are those at the start (north) of the long strips of strongly connected reefs (see figure 5.34).

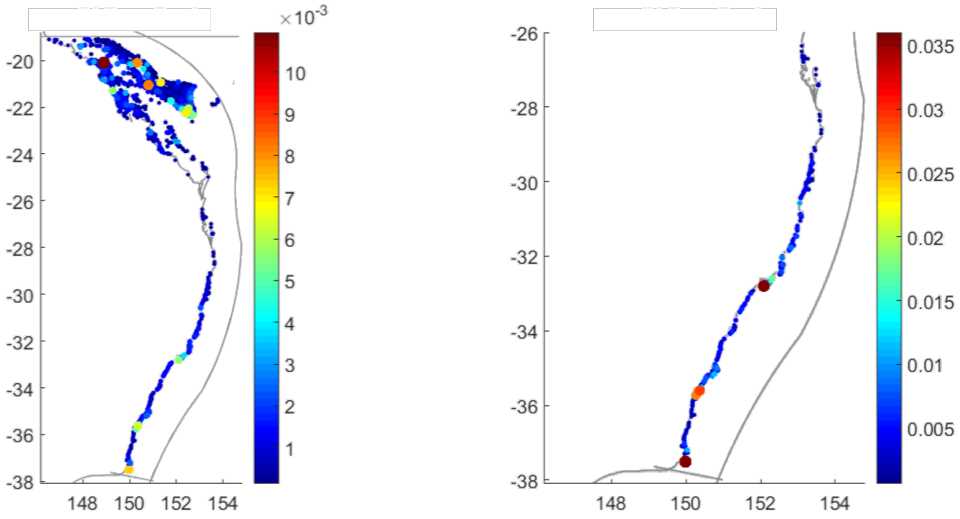

Figure 5.33: The Incoming PageRank index π^{in} in the whole domain and in the southern part.

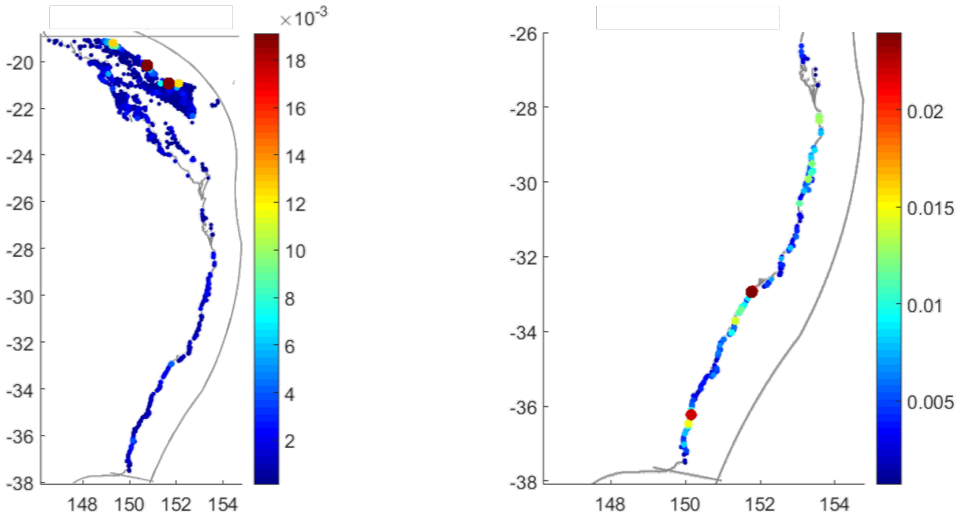

Figure 5.34: The Outcoming PageRank index π^{out} in the whole domain and in the southern part.

5.3 Protection and restoration indices

5.3.1 PageRank protection index

We can observe the same pattern several times along the coast (see figure 5.35). We can distinguish 4 strips of reefs, the longest being the one mentioned several times above. The

reefs at the start of these strips are the ones that needs to be protected first. It seems logical since they provide larvae for all the reefs of the same strip which are further south. At the same time, almost all the larvae that settle on them are their own larvae (see the self recruitment in figure 5.29).

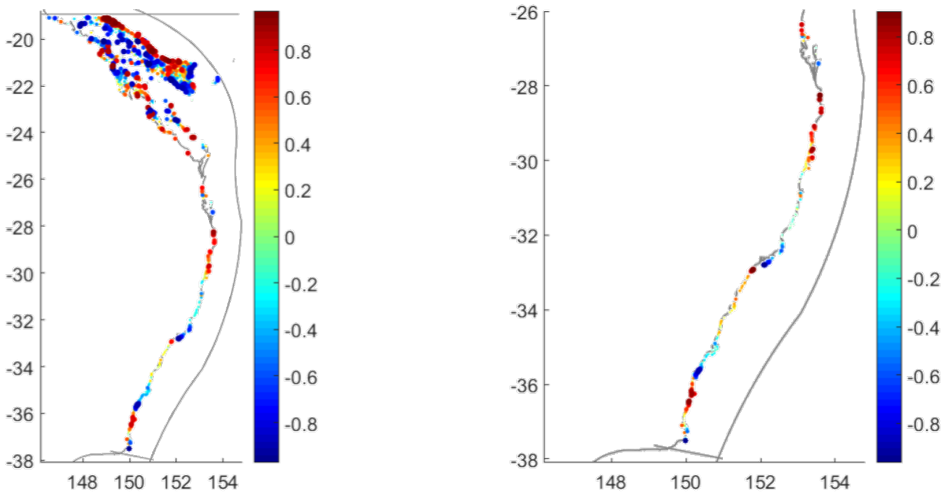

Figure 5.35: The PageRank protection index π^{out-in} in the whole domain and in the southern part.

5.3.2 PageRank restoration index

As you would expect, the points that emerge are mostly located at the middle of these strips (see figure 5.36). Indeed it was said in section 4.3.2 that the reefs that we wanted to restore had to be good importers and exporters. The reefs at the start or the end of the strips do not fulfill both conditions. While the reefs in the middle of this strips receive larvae from the north and send theirs southward.

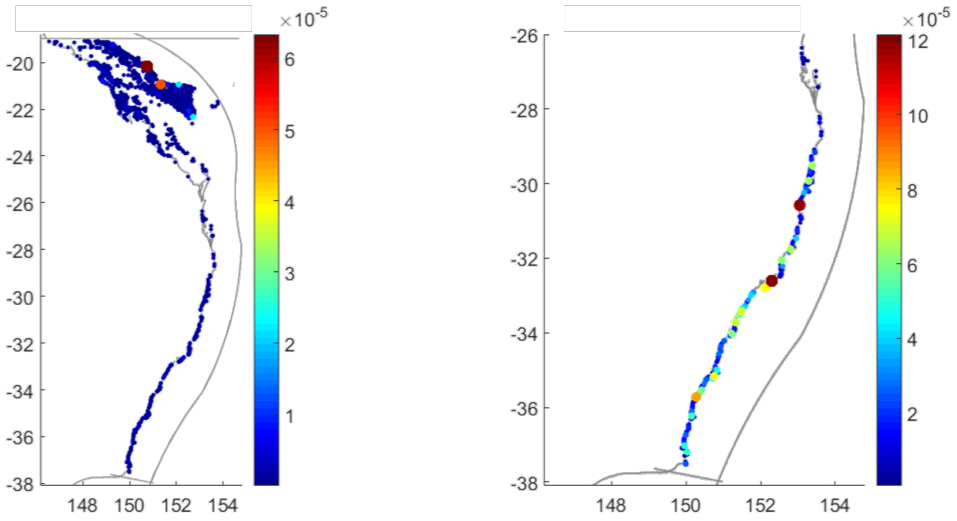

Figure 5.36: The PageRank restoration index $\pi^{out \times in}$ in the whole domain and in the southern part.

5.4 Communities and reef clusters identification

With everything the previous sections taught us in mind, the strongly connected components method seems inadequate. Indeed the connections are for the most part pointing southward. The condition of strong connection is thus a clear obstacle for the southern part. Figure 5.37 proves this theory; only 8 small clusters are highlighted in the southern part. On the GBR side we still have to take the results with caution, especially in the north. However the outer southern part of the GBR on our graph seems to form a substantial cluster, while the reefs closer to the coast are more split in smaller clusters.

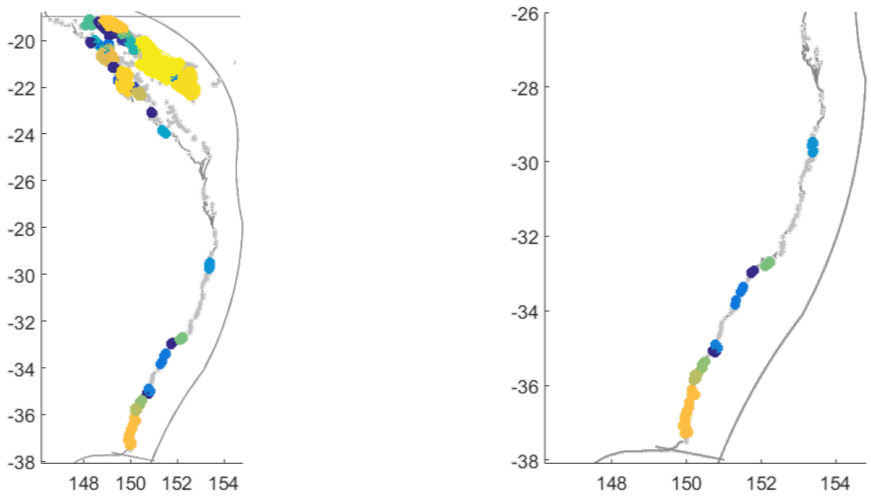

Figure 5.37: The clusters (with the SCC method) in the whole domain and in the southern part.

The "weakly connected components" (WCC) method is a version of the SCC method: instead of considering the strong (in both directions) connections it considers the weak connections (a connection in one direction is enough). However it does not actually show much except the clear-cut separation between the GBR reefs and the southern reefs (see figure 5.38).

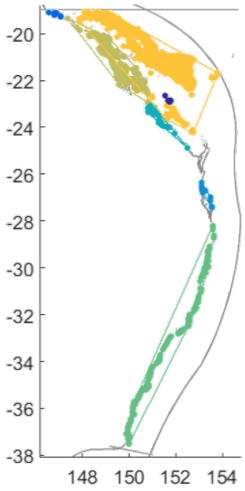

Figure 5.38: The clusters (with the WCC method) in the whole domain.

With more time, it would make sense to look at other methods to establish the clusters differently since the unidirectionality distorts the results.

5.5 Some further thoughts

This study only considered the average of the runs, over a single period. The next step in gathering information on these reefs is surely a further statistical analysis, considering different years.

As said in section 5.4, a different method to identify clusters of reefs would be necessary. Studies like [C. J. Thomas et al. , 2014] have looked into this and models like the constant Potts model (CPM) (developed by [Traag, Van Dooren, and Nesterov , 2011] and [Ronhovde and Nussinov , 2010]) seem to emerge.

The question of the mapping of the reefs is still relevant. We try to analyse the reefs' connectivity and bring out the communities while in fact we neglect some (small) communities by taking treating as a single reef.

6 Conclusion

Through the modeling of A. Millepora larval exchanges, this study intends to guide and give information about subtropical reefs on the east coast of Australia. Biogeographic transition zones get more interesting as the impacts of climate change are more pronounced, frequent and inexorable. Coral bleaching is a perfect example of these impacts when we talk about corals. Sheltering many tropical and temperate species living at the margins of their range, these zones become large natural laboratories, allowing us to get an overview of the reaction of these species to climate change. Since range shifts have already been observed for some tropical coral fishes mainly, scientists are exploring the potential of these subtropical reefs as refuges. In order to learn more about the reefs of this area and especially about their larval exchanges, three main steps had to be achieved.

First we had to simulate to the best of our ability the currents on our domain with a high-resolution ocean model. Among all hydrodynamic models, SLIM was chosen for its superior precision in shallow waters already experienced in other studies. A major feature allowing this fact is the use of an unstructured mesh. Thanks to this we can push the boundaries of our computational domain far enough from the region of interest, making it finer (until 500m) near the coast and reefs and coarser (until 10 km) on deep ocean. A relaxation term towards HYCOM is however introduced, making it more important as one moves away from the coasts and reefs and as the ocean gets deeper.

Afterwards the larval dispersal had to be modelled with a Lagrangian Particle Tracker implemented in SLIM. Biological parameters specific to A. Millepora were introduced in the model and the connectivity matrix was constructed.

We finished with the connectivity matrix analysis, using predefined tools to formulate findings.

The first observation was the absence of exchanges between the GBR and southern reefs. The choice was made to focus on the south part of the domain, little studied so far in comparison with the number of studies about the GBR.

These reefs are under the major influence of the EAC. Since the reefs density is far lower than in the GBR, a good number of reefs are isolated, receiving very few larvae from other reefs than themselves. The best importing reefs are the ones that benefit from the EAC running closer to the coast and bringing more distant reef larvae. The exchanges happen mainly between reefs that are close to each other. They occur from north to south in long strips along the coast. We noticed 4 strips of this type separated by poorer regions in larval exchanges.

The consequence of this particular behavior is that the reefs that need the most protection are the ones at the start of these strips. Indeed we want the reefs we protect to be poor importers of larvae but good exporters. Since they do not get many larvae from the "poorer regions" north to them", but provide their own larvae to a good num-

ber of reefs from the same strip south to them, they are the perfect candidates for protection.

In terms of restoration, theses strips still play a major role. We want the reefs we restore to be both useful to the community, to other reefs and resilient enough to have good chances to survive on their own after the restoration. The best candidates for this are reefs located in the middle of the strips. Indeed half the reefs of the strip are potentially able to provide them in larvae whereas the other half is likely to receive their larvae.

However this whole process is not exempt from errors and approximations, its limitations have been detailed above in this paper. Further works will use a shorter time step and a higher resolution to avoid grouping separate coral reefs into one. We also regret the limited data available to validate our model. The little validation we could get is encouraging without fitting perfectly with reality. Other discussion points have been mentioned such as the real percentage of coral cover on the reef maps or the biological parameters. The latter have been reduced to a minimum with assumptions and there is no doubt that the following works will model the coral larvae behavior closer to reality.

Some courses of action have also been recommanded such as another method to identify reef clusters.

In the present context there is no doubt that this study simply laid the preliminary foundations in all that could and will be done about these subtropical coral reefs. Hopefully all the contributions to this cause will allow to preserve these wonderful endangered ecosystems that are coral reefs.

References

Amante, C., & Eakins, B. W. (n.d.). Etopo1 arc-minute global relief model: procedures, data sources and analysis. *Test*.

Andutta, F. P., Ridd, P. V., & Wolanski, E. (2011). Dynamics of hypersaline coastal waters in the great barrier reef. *Estuarine, Coastal and Shelf Science*, *94*(4), 299–305.

Bechet, V., & Verstraeten, E. (2018). *Multiple-year marine connectivity modeling in the florida coral reef tract to assess acropora cervicornis recovery* (Unpublished master's thesis). Ecole polytechnique de Louvain, Université catholique de Louvain, 2018. Faculté des bioingénieurs, Université catholique de Louvain, 2018. (Prom. : Hanert, Emmanuel ; Deleersnijder, Eric.)

Beger, M., Sommer, B., Harrison, P. L., Smith, S. D., & Pandolfi, J. M. (2014). Conserving potential coral reef refuges at high latitudes. *Diversity and distributions*, *20*(3), 245–257.

Bleck, R. (2002). An oceanic general circulation model framed in hybrid isopycnic-cartesian coordinates. *Ocean modelling*, *4*(1), 55–88.

Booth, D. J., & Sear, J. (2018). Coral expansion in sydney and associated coral-reef fishes. *Coral Reefs*, *37*(4), 995–995.

Carpenter, K. E., Abrar, M., Aeby, G., Aronson, R. B., Banks, S., Bruckner, A., ... others (2008). One-third of reef-building corals face elevated extinction risk from climate change and local impacts. *Science*, *321*(5888), 560–563.

Chassignet, E. P., Hurlburt, H. E., Smedstad, O. M., Halliwell, G. R., Hogan, P. J., Wallcraft, A. J., ... Bleck, R. (2007). The hycom (hybrid coordinate ocean model) data assimilative system. *Journal of Marine Systems*, *65*(1-4), 60–83.

Connolly, S. R., & Baird, A. H. (2010). Estimating dispersal potential for marine larvae: dynamic models applied to scleractinian corals. *Ecology*, *91*(12), 3572–3583.

Costanza, R., d'Arge, R., De Groot, R., Farber, S., Grasso, M., Hannon, B., ... others (1997). The value of the world's ecosystem services and natural capital. *nature*, *387*(6630), 253-260.

Cushman-Roisin, B., & Beckers, J.-M. (2011). *Introduction to geophysical fluid dynamics: physical and numerical aspects* (Vol. 101). Academic press.

De Brye, B., de Brauwere, A., Gourgue, O., Kärnä, T., Lambrechts, J., Comblen, R., & Deleersnijder, E. (2010). A finite-element, multi-scale model of the scheldt tributaries, river, estuary and rofi. *Coastal Engineering*, *57*(9), 850–863.

de Brye, B., Schellen, S., Sassi, M., Vermeulen, B., Kärnä, T., Deleersnijder, E., & Hoitink, T. (2011). Preliminary results of a finite-element, multi-scale model of the mahakam delta (indonesia). *Ocean Dynamics*, *61*(8), 1107–1120.

Dobbelaere, T. (2018). *Numerical study of whitings formation on the bahama bank* (Unpublished master's thesis). Ecole polytechnique de Louvain, Université catholique de Louvain, 2018. (Prom. : Hanert, Emmanuel ; Deleersnijder, Eric.)

Egbert, G. D., & Erofeeva, S. Y. (2002). Efficient inverse modeling of barotropic ocean

tides. *Journal of Atmospheric and Oceanic Technology*, *19*(2), 183–204.

Ferrario, F., Beck, M. W., Storlazzi, C. D., Micheli, F., Shepard, C. C., & Airoldi, L. (2014). The effectiveness of coral reefs for coastal hazard risk reduction and adaptation. *Nature communications*, *5*(3794).

Figueiredo, J., Baird, A. H., & Connolly, S. R. (2013). Synthesizing larval competence dynamics and reef-scale retention reveals a high potential for self-recruitment in corals. *Ecology*, *94*(3), 650–659.

Frys, C. (2018). *Modeling marine connecivity in the florida coral reef tract* (Unpublished master's thesis). Faculté des bioingénieurs, Université catholique de Louvain, 2018. (Prom. : Hanert, Emmanuel.)

Geernaert, G. (1987). On the importance of the drag coefficient in air-sea interactions. *Dynamics of Atmospheres and Oceans*, *11*(1), 19–38.

Hamon, B. (1965). The east australian current, 1960–1964. In *Deep sea research and oceanographic abstracts* (Vol. 12, pp. 899–921).

Hanert, E., Thomas, C., Lambrechts, J., Deleersnijder, E., & Wolanski, E. (2012). Studying coral reefs connectivity using slim and tools from graph theory. In *11th international workshop on unstructured mesh numerical modelling of coastal, shelf and ocean flows.*

Hannam, P. (2018). Sydney's marine life turning troppo as coral, other species head south. *The Sydney Morning Herald (website).*

Harriott, V. (1999). Coral growth in subtropical eastern australia. *Coral Reefs*, *18*(3), 281–291.

Hata, T., Madin, J. S., Cumbo, V. R., Denny, M., Figueiredo, J., Harii, S., ... Baird, A. H. (2017). Coral larvae are poor swimmers and require fine-scale reef structure to settle. *Scientific reports*, *7*(1), 2249.

Hoegh-Guldberg, O. (1999). Climate change, coral bleaching and the future of the world's coral reefs. *Marine and freshwater research*, *50*(8), 839–866.

Hughes, T. P., Anderson, K. D., Connolly, S. R., Heron, S. F., Kerry, J. T., Lough, J. M., ... others (2018). Spatial and temporal patterns of mass bleaching of corals in the anthropocene. *Science*, *359*(6371), 80–83.

Hughes, T. P., Baird, A. H., Bellwood, D. R., Card, M., Connolly, S. R., Folke, C., ... others (2003). Climate change, human impacts, and the resilience of coral reefs. *science*, *301*(5635), 929–933.

Hunter, J., Craig, P., & Phillips, H. (1993). On the use of random walk models with spatially variable diffusivity. *Journal of Computational Physics*, *106*(2), 366–376.

Lambrechts, J., Hanert, E., Deleersnijder, E., Bernard, P.-E., Legat, V., Remacle, J.-F., & Wolanski, E. (2008). A multi-scale model of the hydrodynamics of the whole great barrier reef. *Estuarine, Coastal and Shelf Science*, *79*(1), 143–151.

Makino, A., Yamano, H., Beger, M., Klein, C. J., Yara, Y., & Possingham, H. P. (2014). Spatio-temporal marine conservation planning to support high-latitude coral range expansion under climate change. *Diversity and Distributions*, *20*(8), 859–871.

Okubo, A. (1971). Oceanic diffusion diagrams. In *Deep sea research and oceanographic abstracts* (Vol. 18, pp. 789–802).

Page, L., Brin, S., Motwani, R., & Winograd, T. (1999). *The pagerank citation ranking: Bringing order to the web.* (Tech. Rep.). Stanford InfoLab.

Ronhovde, P., & Nussinov, Z. (2010). Local resolution-limit-free potts model for community detection. *Physical Review E*, *81*(4), 046114.

Smagorinsky, J. (1963). General circulation experiments with the primitive equations: I. the basic experiment. *Monthly weather review*, *91*(3), 99–164.

Smith, S., & Banke, E. (1975). Variation of the sea surface drag coefficient with wind

speed. *Quarterly Journal of the Royal Meteorological Society*, *101*(429), 665–673.

Smith, W. H., & Sandwell, D. T. (1997). Global sea floor topography from satellite altimetry and ship depth soundings. *Science*, *277*(5334), 1956–1962.

Sommer, B., Harrison, P. L., Beger, M., & Pandolfi, J. M. (2014). Trait-mediated environmental filtering drives assembly at biogeographic transition zones. *Ecology*, *95*(4), 1000–1009.

Spagnol, S., Wolanski, E., Deleersnijder, E., Brinkman, R., McAllister, F., Cushman-Roisin, B., & Hanert, E. (2002). An error frequently made in the evaluation of advective transport in two-dimensional lagrangian models of advection-diffusion in coral reef waters. *Marine Ecology Progress Series*, *235*, 299–302.

Stanley, G. D. (2006). Photosymbiosis and the evolution of modern coral reefs. *Science*, *312*(5775), 857–858.

Thomas, C. (2015). *Modelling marine connectivity in the great barrier reef and exploring its ecological implications* (Unpublished doctoral dissertation). Doctoral dissertation, UCL.

Thomas, C. J., Lambrechts, J., Wolanski, E., Traag, V. A., Blondel, V. D., Deleersnijder, E., & Hanert, E. (2014). Numerical modelling and graph theory tools to study ecological connectivity in the great barrier reef. *Ecological Modelling*, *272*, 160–174.

Traag, V. A., Van Dooren, P., & Nesterov, Y. (2011). Narrow scope for resolution-limit-free community detection. *Physical Review E*, *84*(1), 016114.

Van, C. P., Gourgue, O., Sassi, M., Hoitink, A., Deleersnijder, E., & Soares-Frazão, S. (2016). Modelling fine-grained sediment transport in the mahakam land–sea continuum, indonesia. *Journal of hydro-environment research*, *13*, 103–120.

Webster, M., & Petkovic, P. (2005). Australian bathymetry and topography grid. *Geoscience Australia*.

Whiteway, T. (2009). Australian bathymetry and topography grid. *Geoscience Australia, Canberra*.

Yoon, T. H., & Kang, S.-K. (2004). Finite volume model for two-dimensional shallow water flows on unstructured grids. *Journal of Hydraulic Engineering*, *130*(7), 678–688.

A Appendices

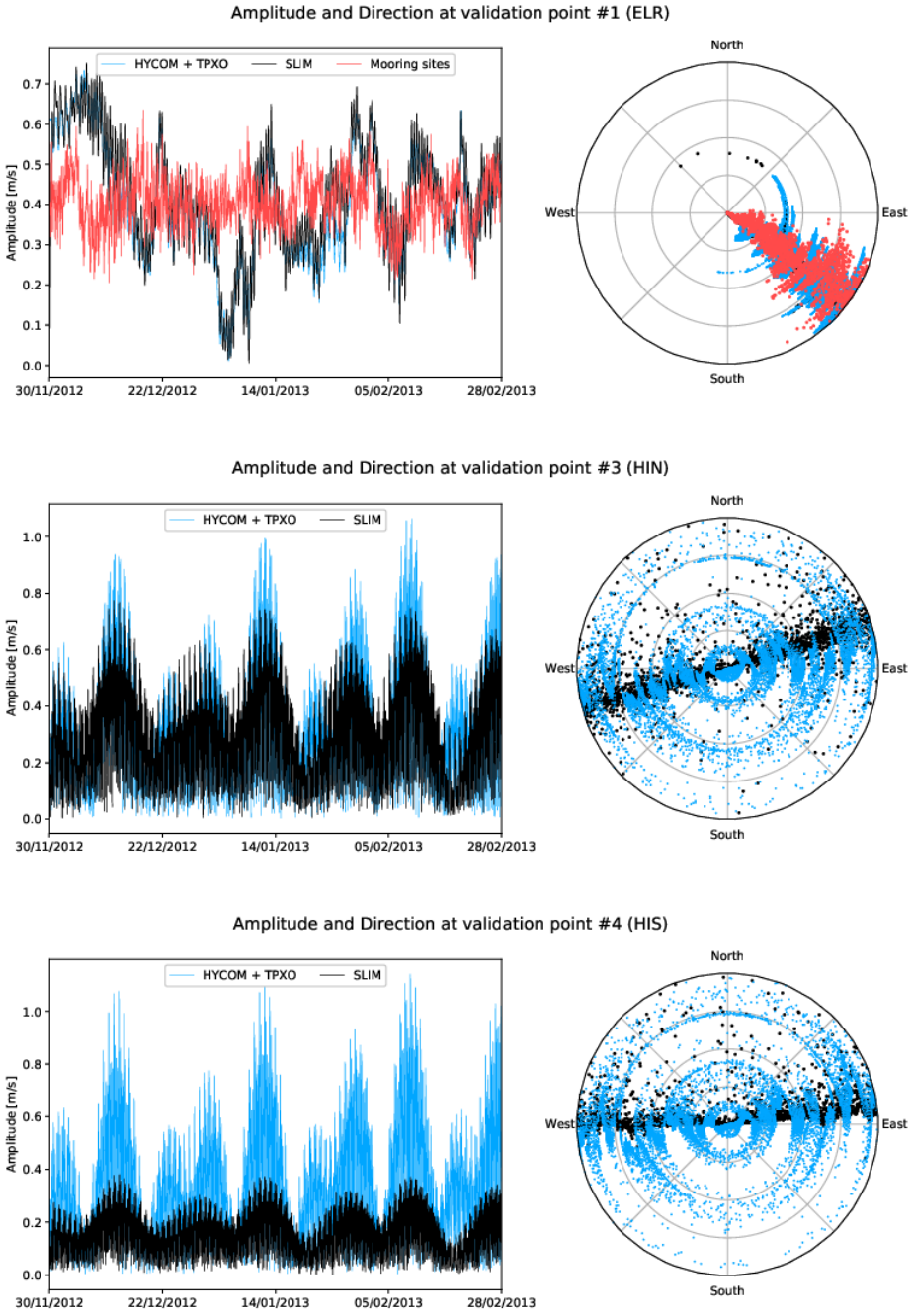

Figure 1.39: The validation graph of the velocities of points 1, 3 and 4.

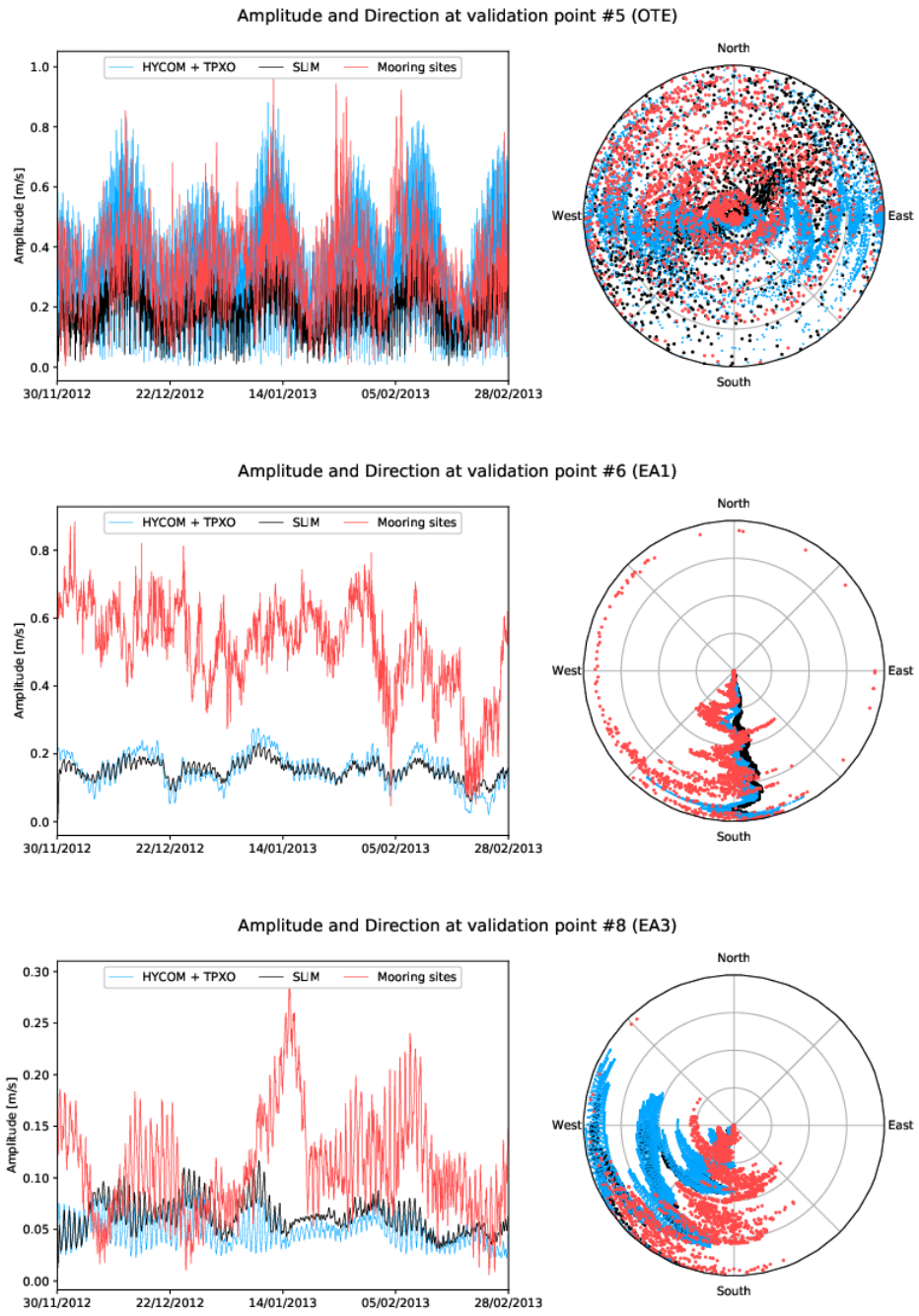

Figure 1.40: The validation graph of the velocities of points 5, 6 and 8.

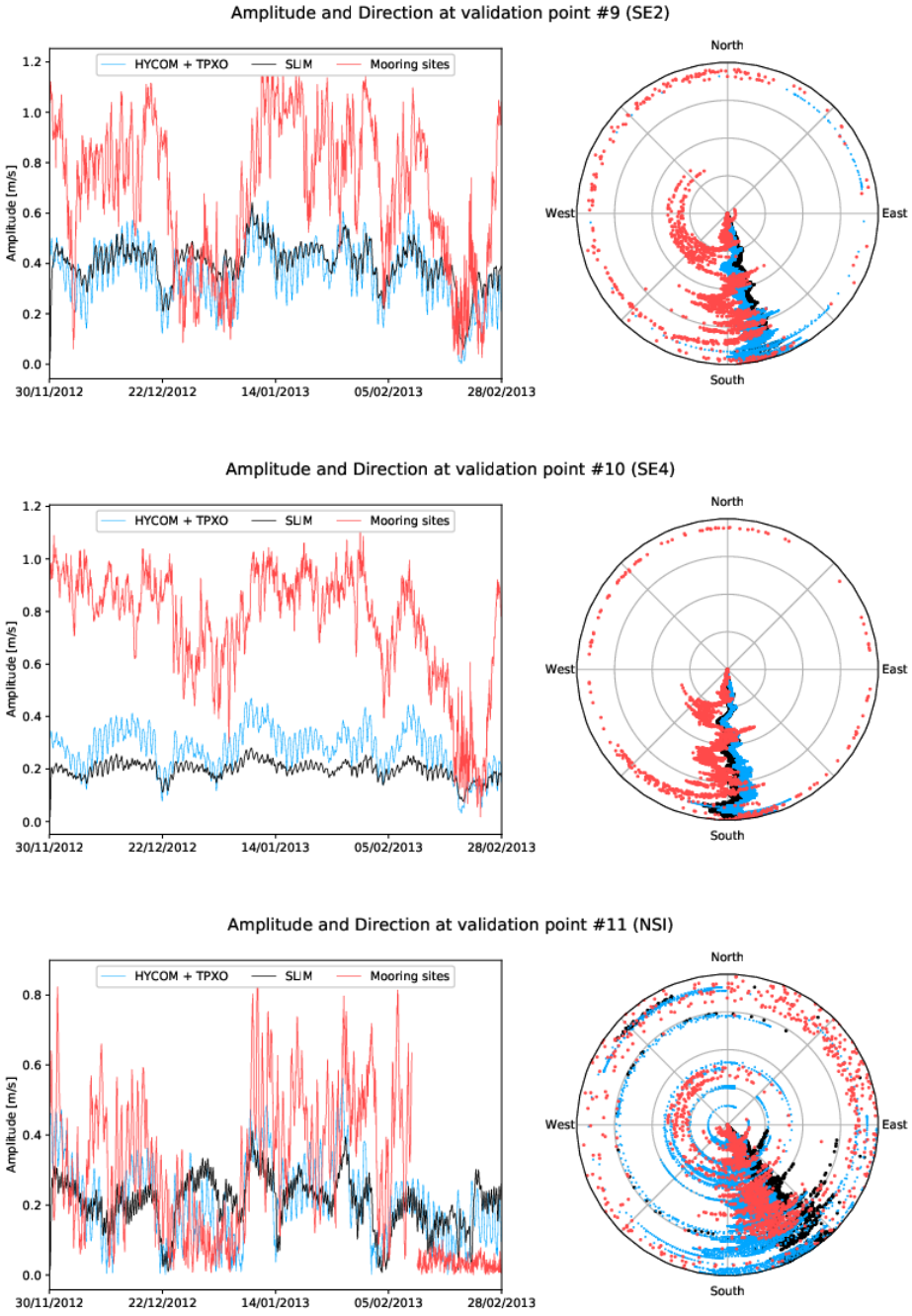

Figure 1.41: The validation graph of the velocities of points 9, 10 and 11.

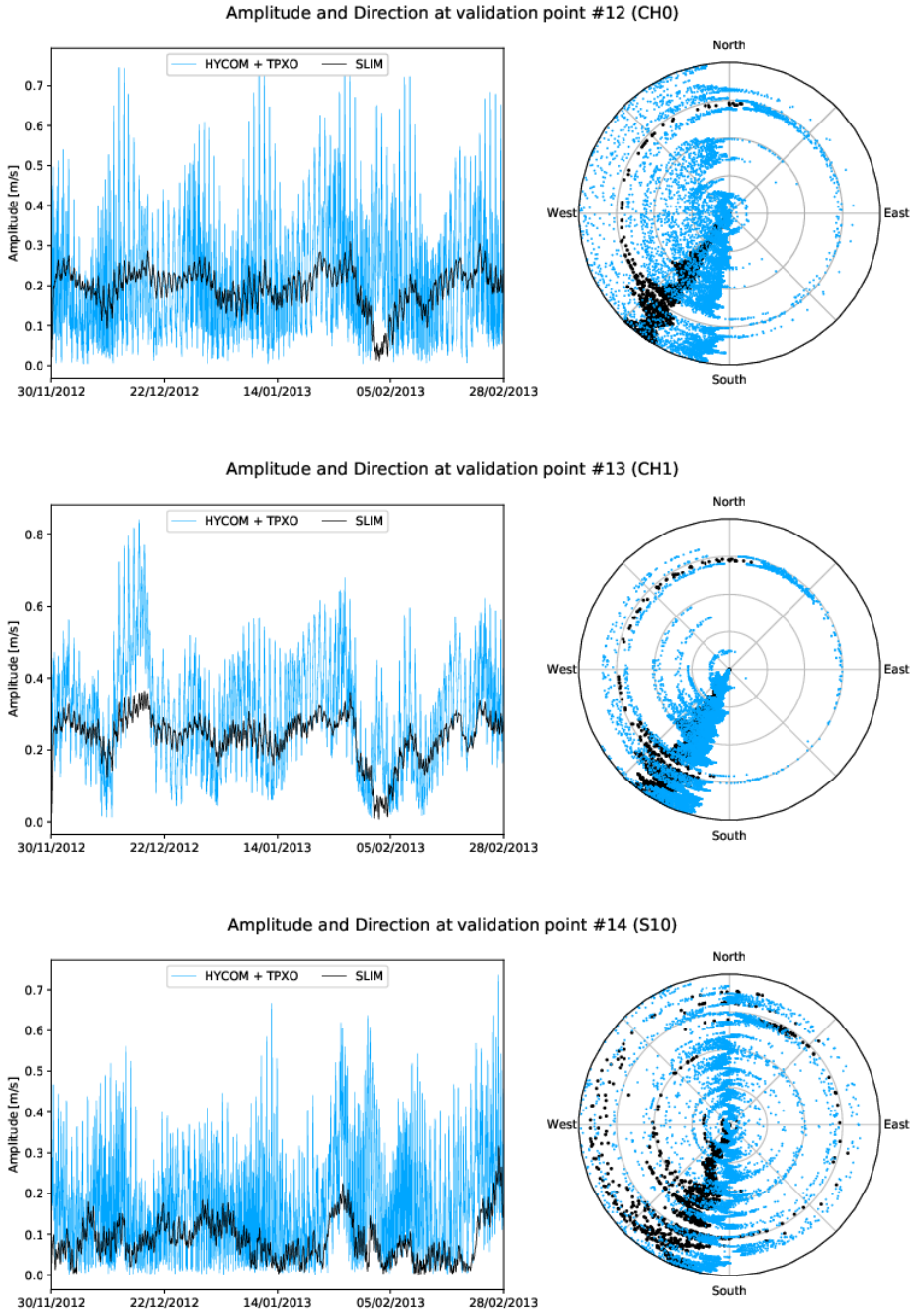

Figure 1.42: The validation graph of the velocities of points 12, 13 and 14.

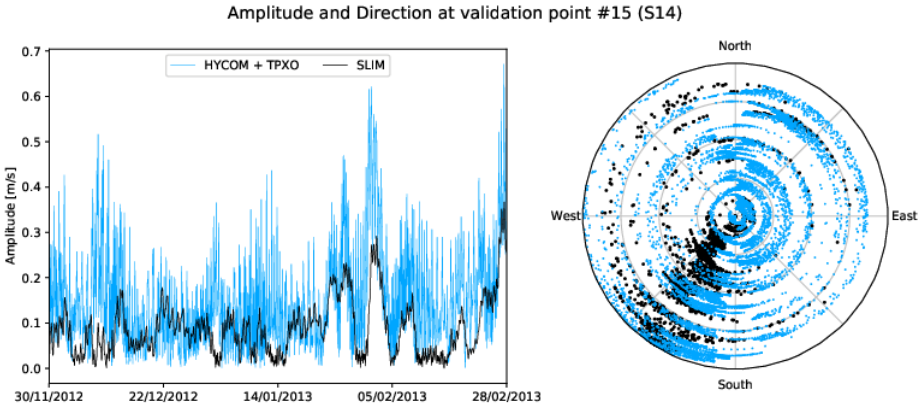

Figure 1.43: The validation graph of the velocities of point 15.

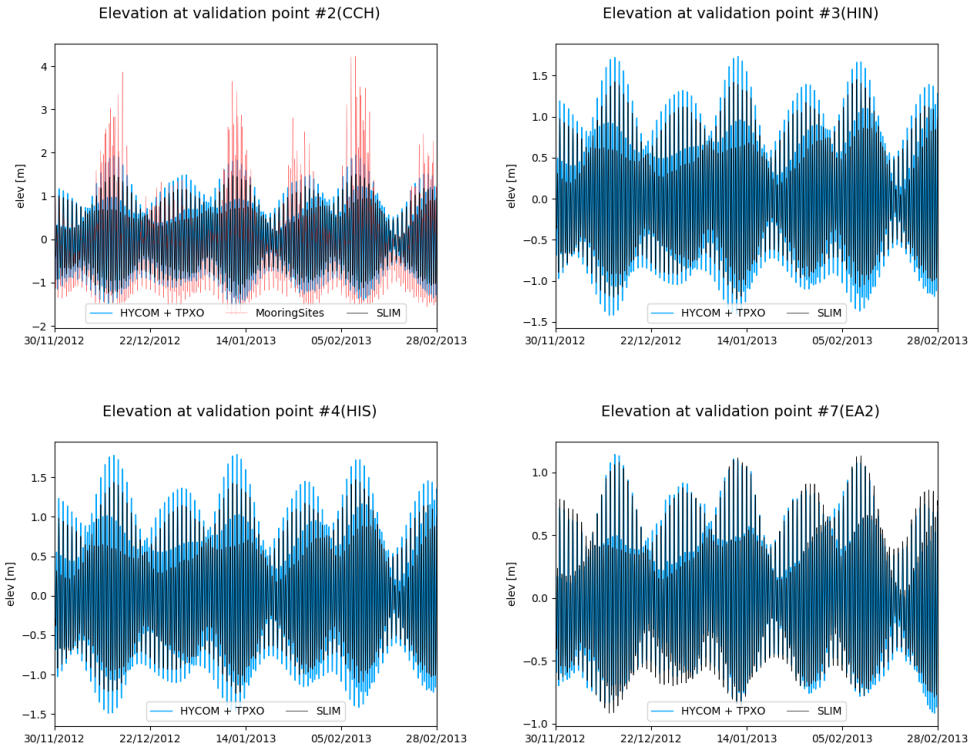

Figure 1.44: The validation graph of the elevation of points 2, 3, 4 and 7.

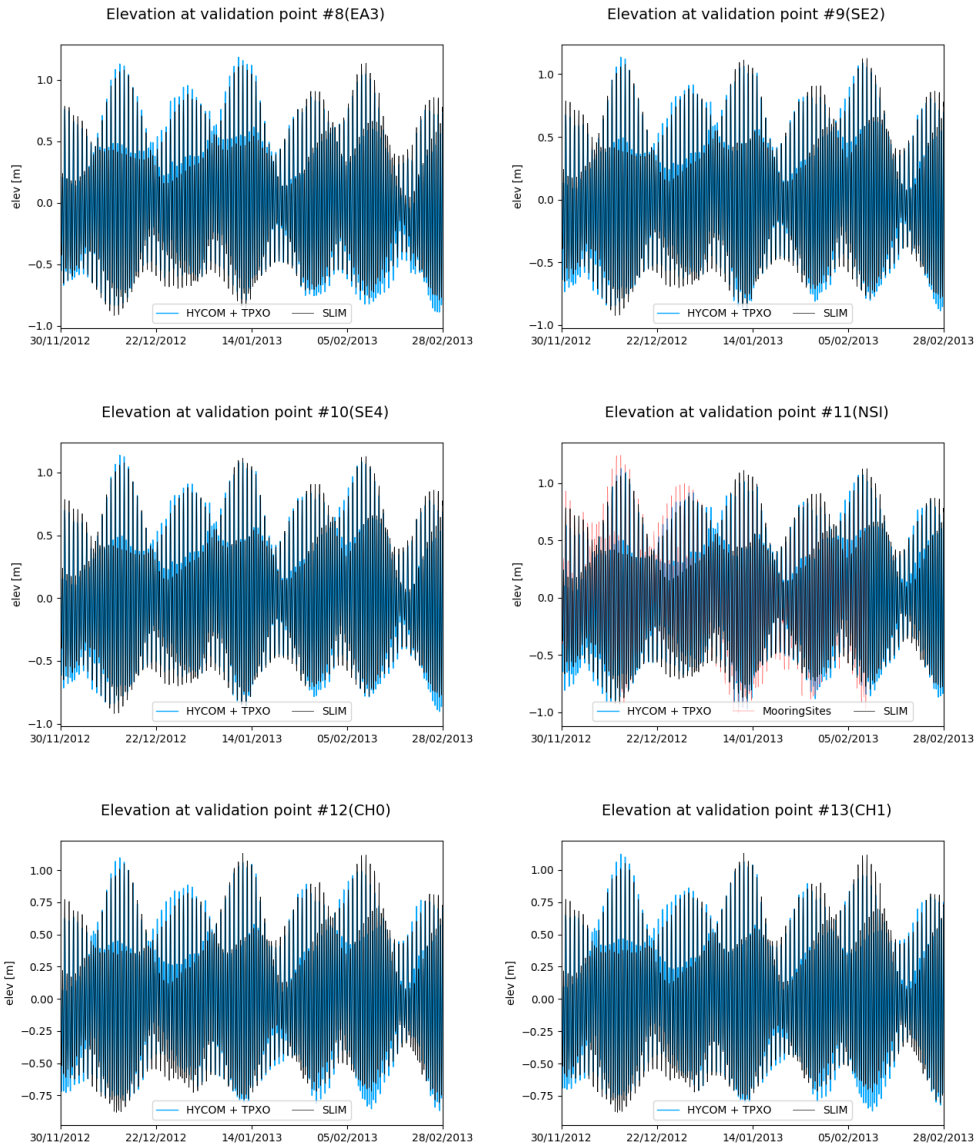

Figure 1.45: The validation graph of the elevation of points 8,9,10,11,12 and 13.

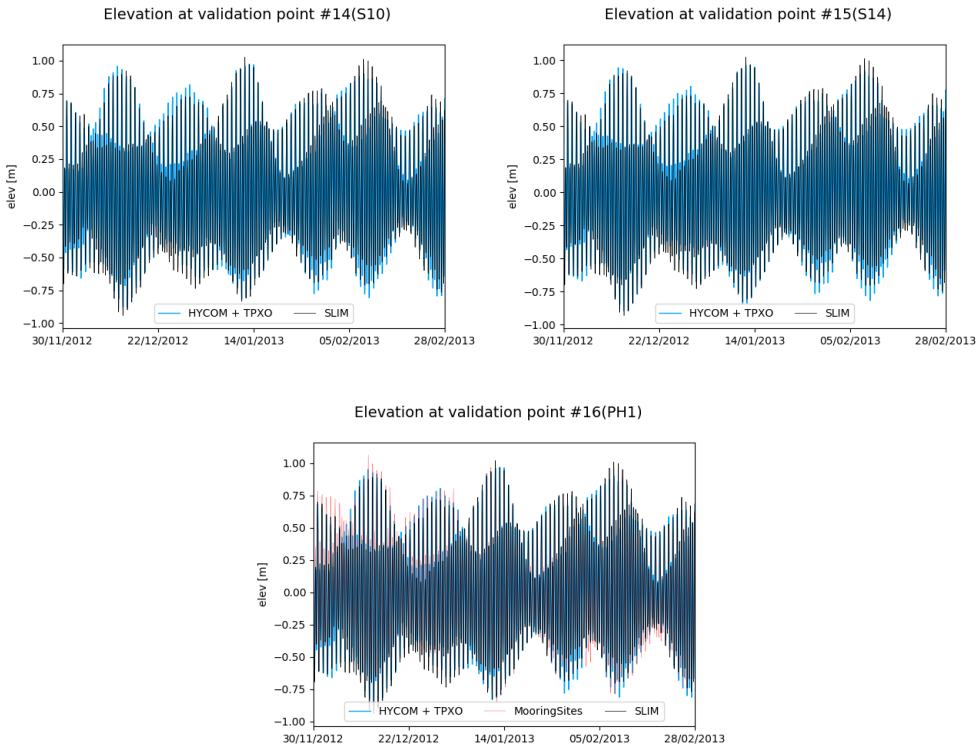

Figure 1.46: The validation graph of the elevation of points 14, 15 and 16.

UNIVERSITÉ CATHOLIQUE DE LOUVAIN
École polytechnique de Louvain
Rue Archimède, 1 bte L6.11.01, 1348 Louvain-la-Neuve, Belgique | **www.uclouvain.be/epl**